

Space-Time Spectral Collocation Tensor Network Approach for Maxwell's Equations

Dibyendu Adak^{a,b}, Rujeko Chinomona^a, Duc P. Truong^a, Oleg Korobkin^a, Kim Ø. Rasmussen^a, Boian S. Alexandrov^a

^a*Theoretical Division, Los Alamos National Laboratory, Los Alamos, NM 87545, USA*

^b*Indian Institute of Technology-Kharagpur, WB, India*

Abstract

In this work, we develop a space–time Chebyshev spectral collocation method for three-dimensional Maxwell's equations and combine it with tensor-network techniques in Tensor-Train (TT) format. Under constant material parameters, the Maxwell system is reduced to a vector wave equation for the electric field, which we discretize globally in space and time using a staggered spectral collocation scheme. The staggered polynomial spaces are designed so that the discrete curl and divergence operators preserve the divergence-free constraint on the magnetic field. The magnetic field is then recovered in a space–time post-processing step via a discrete version of Faraday's law. The global space–time formulation yields a large but highly structured linear system, which we approximate in low-rank TT-format directly from the operator and data, without assuming that the forcing is separable in space and time. We derive condition-number bounds for the resulting operator and prove spectral convergence estimates for both the electric and magnetic fields. Numerical experiments for three-dimensional electromagnetic test problems confirm the theoretical convergence rates and show that the TT-based solver maintains accuracy with approximately linear complexity in the number of grid points in space and time.

1. Introduction

The accurate and efficient numerical solution of Maxwell's equations remains a cornerstone challenge in computational electromagnetics, with applications spanning satellite communications, medical imaging, radar systems, telecommunication devices, and numerous other technologies critical to modern society. Maxwell's equations describe the propagation and scattering of electromagnetic waves, and their time-dependent nature requires careful treatment to preserve physical properties while maintaining computational efficiency. As electromagnetic devices and systems become increasingly complex and operate at higher frequencies, the demand for high-fidelity simulations that can resolve fine-scale features across large computational domains has grown substantially.

Many numerical approaches for time-dependent partial differential equations combine spectral methods for spatial discretization with low-order finite difference schemes for temporal discretization [17]. While spectral methods offer exponential convergence for smooth solutions in the spatial domain, this advantage is undermined when temporal errors dominate, reducing the overall convergence to first or second order. To address this limitation, space-time spectral collocation methods have been developed [23, 22, 24], where both spatial and temporal dimensions are discretized using high-order spectral approximations. These methods achieve exponential convergence globally but require solving for all time steps simultaneously, substantially increasing the dimensionality of the problem and introducing significant computational challenges.

For Maxwell's equations specifically, preserving the divergence-free constraint of the magnetic field ($\nabla \cdot \mathbf{B} = 0$) poses a fundamental numerical challenge. Classical approaches have addressed this through various means. Yee's pioneering finite-difference time-domain scheme [39] introduced spatial staggering of field components on a Cartesian grid, a principle that has been extended to fourth-order accurate compact schemes [40, 41]. Discontinuous Galerkin methods [3, 6] and multidomain methods [7] have also been developed to maintain divergence-free properties while allowing for complex geometries and material interfaces. In the spectral element context, Monk [28] analyzed finite element discretizations of Maxwell's equations, while more recent work has explored Legendre-tau Chebyshev collocation spectral element methods with Runge-Kutta time integration [29] and divergence-free finite element schemes for static problems [16]. Despite these advances, the computational cost of these methods remains substantial, particularly for three-dimensional problems requiring fine resolution over long time intervals.

A more fundamental obstacle confronts all traditional approaches to solving Maxwell's equations in three spatial dimensions plus time: the curse of dimensionality [5]. The number of degrees of freedom grows exponentially with dimension, rendering fine-resolution simulations prohibitively expensive or entirely infeasible. Consider, for example, full waveform inversion problems in geophysics or radar imaging, where the number of grid points per time step can reach $M = 10^9$ or more [20]. With N time steps required to simulate the wave propagation, one must store and manipulate MN floating point numbers, quickly exceeding available memory even on modern high-performance computing systems. This exponential scaling defeats traditional computational approaches and forces difficult trade-offs. One option is to employ reduced-order models (ROMs) [14, 21, 8], which construct low-dimensional approximations of the solution manifold. While ROMs excel for certain problem classes, they often require significant domain expertise, are tailored to specific applications, and demand invasive modifications to existing simulation codes. Another option is checkpointing, where only selected time steps are stored and intermediate states are recomputed as needed, but this approach multiplies the computational cost and still faces memory limitations for large-scale problems.

Tensor network methods have emerged as a promising alternative for mitigating the curse of dimensionality in high-dimensional problems. These methods exploit the observation that many high-dimensional functions of practical interest, despite having exponentially many degrees of freedom in principle, can be well approximated by low-rank tensor decompositions. Among tensor formats, the tensor-train (TT) decomposition introduced by Oseledets [32] has gained widespread adoption because it can accurately represent complex functions while remaining computationally feasible. The TT format represents a d -dimensional tensor as a product of three-dimensional cores, effectively implementing a discrete separation of variables [4]. Crucially, when the underlying function admits a low-rank structure, the TT representation achieves linear complexity in both storage and computation with respect to dimension and discretization level. This strongly contrasts the exponential scaling of conventional methods.

The utility of tensor-train methods rests on efficient algorithms that can construct and manipulate TT representations without ever forming the full tensor. The TT-cross interpolation algorithm [31, 35, 37] addresses the construction problem by adaptively selecting tensor fibers that capture the essential structure, building the decomposition from carefully chosen one-dimensional slices rather than the complete high-dimensional array. For solving linear systems in TT format, alternating optimization methods [33, 10, 15] have proven effective, iteratively updating each core while fixing the others. These algorithms have been successfully applied to quantum many-body problems, chemical master equations, and various PDE systems. Moreover, the Quantized Tensor-Train format [18] provides additional compression for operators with special structure, such as the banded matrices arising from spectral discretizations.

Recent work has begun to explore the combination of tensor network methods with high-order

discretizations for PDEs. Applications include the Boltzmann neutron transport equation [38], where the TT format enables simulations in the full six-dimensional phase space; the mimetic finite difference method for Maxwell's equations [26]; and space-time spectral collocation for nonlinear convection-diffusion equations [1, 2], where the TT approach has demonstrated dramatic computational savings while preserving spectral accuracy. These successes suggest that tensor methods may offer a path forward for large-scale electromagnetic simulations that would be intractable with conventional approaches.

In this work, we develop a novel space-time spectral collocation method for Maxwell's equations that leverages tensor-train decomposition to overcome the curse of dimensionality while maintaining exponential convergence. Our approach begins with a global space-time formulation where both spatial and temporal dimensions are discretized using Chebyshev-Gauss-Lobatto collocation points. This yields a large block-structured linear system that encapsulates the entire time evolution, making all time steps available simultaneously for tensor compression. Under the assumption of constant material parameters, we reformulate Maxwell's system as a vector wave equation for the electric field [28], allowing us to solve for each electric field component independently. The magnetic field is then recovered through post-processing using a discretization of Faraday's law. To preserve the divergence-free property of the magnetic field without explicit constraint enforcement, we use a spectral analogue of classical staggered grids: electric and magnetic field components live in different polynomial spaces with carefully chosen degrees of freedom in each coordinate direction. This spectral staggering ensures that the discrete curl operator maps between compatible spaces and that the discrete identity $\nabla \cdot (\nabla \times \cdot) \approx 0$ holds to spectral accuracy.

The Kronecker product structure of the discrete operators arising from this space-time formulation proves naturally compatible with tensor-train representations. Each spatial and temporal derivative operator can be expressed as a Kronecker product of one-dimensional matrices, and the resulting discrete wave equation inherits this structure. We construct TT representations of the solution, operators, and boundary data using TT-cross interpolation, solving the compressed system using alternating minimal energy methods [10]. The theoretical analysis establishes rigorous foundations for the method, including condition number estimates showing $\mathcal{O}(N^4)$ scaling for the wave operator and $\mathcal{O}(N^2)$ scaling for the temporal operator, as well as proofs of exponential convergence for both electric and magnetic fields. We also prove that both Gauss's law for the electric field and the divergence-free constraint for the magnetic field are satisfied with exponential accuracy.

Numerical experiments validate these theoretical results and demonstrate the practical efficiency of the method. Across test cases with manufactured solutions of varying tensor rank, we consistently observe exponential convergence matching the full-grid spectral method while achieving computational speedups of 10^7 to 10^8 for problems with approximately 2×10^5 space-time degrees of freedom. Critically, the tensor-train method extends well beyond the memory limitations of full-grid computation, successfully handling discretizations that would be completely intractable with conventional approaches.

Our paper is organized as follows. Section 2 introduces the mathematical model, derives the second-order formulation for the electric field, and presents the space-time Chebyshev spectral collocation discretization with staggered spaces. Section 3 develops the matrix formulation of the wave equation and describes the magnetic field reconstruction via post-processing. Section 4 establishes condition number estimates and spectral convergence rates for both electric and magnetic fields. Section 5 reviews tensor network concepts and describes the tensorization procedure for both the electric field solution and magnetic field recovery. Section 6 presents numerical experiments demonstrating exponential convergence and computational speedups compared to full-grid methods. Section 7 offers concluding remarks and discusses future directions. Appendix A provides technical details on the construction of mapping operators and boundary tensors.

2. Mathematical model and discretization

Let $\Omega \subset \mathbb{R}^3$ be a cubic domain with boundary $\partial\Omega$. We consider Maxwell's equations on Ω for the electric field $\mathbf{E} = (E_x, E_y, E_z)$ and the magnetic flux density $\mathbf{B} = (B_x, B_y, B_z)$:

$$\frac{\partial \mathbf{B}}{\partial t} = -\nabla \times \mathbf{E} \quad \text{in } \Omega, \quad \forall t \in (0, T], \quad (2.1)$$

$$\frac{\partial \mathbf{E}}{\partial t} = c^2 \nabla \times \mathbf{B} - \frac{1}{\epsilon_0} \mathbf{J} \quad \text{in } \Omega, \quad \forall t \in (0, T], \quad (2.2)$$

$$\nabla \cdot \mathbf{E} = \rho \quad \text{in } \Omega, \quad (2.3)$$

$$\nabla \cdot \mathbf{B} = 0 \quad \text{in } \Omega, \quad (2.4)$$

where \mathbf{J} is the current density, ρ the charge density, ϵ_0 the dielectric constant, and c the speed of light. We consider the model problem (2.1)–(2.4) with initial conditions $\mathbf{E}(0, \cdot) = \mathbf{E}^0$, $\mathbf{B}(0, \cdot) = \mathbf{B}^0$ and inhomogeneous boundary conditions for both the electric field \mathbf{E} and the magnetic field \mathbf{B} . The implementation of inhomogeneous boundary conditions for the wave equation is not straightforward and will be discussed in detail in Section 3.

Following [28], we can eliminate \mathbf{B} from (2.1)–(2.2) and obtain a second-order equation solely in terms of the electric field. Taking the time derivative of (2.2) and using (2.1) yields

$$\frac{\partial^2 \mathbf{E}}{\partial t^2} + c^2 (\nabla \times \nabla \times \mathbf{E}) = -\frac{1}{\epsilon_0} \frac{d\mathbf{J}}{dt}. \quad (2.5)$$

Using the vector identity $\nabla \times \nabla \times \mathbf{E} = \nabla(\nabla \cdot \mathbf{E}) - \Delta \mathbf{E}$ and substituting (2.3) into (2.5) we obtain the vector wave equation

$$\frac{\partial^2 \mathbf{E}}{\partial t^2} - c^2 \Delta \mathbf{E} = -c^2 \nabla \rho - \frac{1}{\epsilon_0} \frac{d\mathbf{J}}{dt}. \quad (2.6)$$

In this work we assume that the material parameters are constant scalars (so that c and ϵ_0 do not depend on space or time). Under this assumption, the Maxwell system (2.1)–(2.4) reduces to the vector wave equation (2.6) for the electric field, which can be treated componentwise. This form is particularly convenient for the space–time spectral collocation and staggered-grid discretization developed in the remainder of the paper, since it allows us to compute \mathbf{E} explicitly by solving a wave equation in space–time. The magnetic field \mathbf{B} is then recovered from \mathbf{E} in a post-processing step using a discrete form of Faraday's law on a staggered grid (see Sections 2.3 and 3.1). We emphasize that if the coefficients are not constant, the decoupling leading to (2.6) is not straightforward; in that case one would need to work directly with the curl–curl formulation (2.5) and appropriate post-processing on staggered spaces.

Writing (2.6) componentwise, we obtain

$$\frac{\partial^2 E_x}{\partial t^2} - c^2 \Delta E_x = -c^2 \frac{\partial \rho}{\partial x} - \frac{1}{\epsilon_0} \frac{d J_x}{dt}, \quad (2.7)$$

$$\frac{\partial^2 E_y}{\partial t^2} - c^2 \Delta E_y = -c^2 \frac{\partial \rho}{\partial y} - \frac{1}{\epsilon_0} \frac{d J_y}{dt}, \quad (2.8)$$

$$\frac{\partial^2 E_z}{\partial t^2} - c^2 \Delta E_z = -c^2 \frac{\partial \rho}{\partial z} - \frac{1}{\epsilon_0} \frac{d J_z}{dt}, \quad (2.9)$$

which are the scalar wave equations we discretize in space–time in Sections 2.1 and 2.2.

For later use, we also rewrite (2.1) in decoupled form,

$$\begin{aligned}\frac{\partial B_x}{\partial t} &= -\frac{\partial E_z}{\partial y} + \frac{\partial E_y}{\partial z}, \\ \frac{\partial B_y}{\partial t} &= +\frac{\partial E_z}{\partial x} - \frac{\partial E_x}{\partial z}, \\ \frac{\partial B_z}{\partial t} &= -\frac{\partial E_y}{\partial x} + \frac{\partial E_x}{\partial y},\end{aligned}\tag{2.10}$$

which will be the basis for reconstructing \mathbf{B} from the discrete electric field via the post-processing procedures in Sections 2.3 and 3.1.

Further, we will employ the following notation throughout the text. Let $\Omega_X, \Omega_Y, \Omega_Z \subset \mathbb{R}$ be intervals, and define the spatial computational domain

$$\Omega_{\text{space}} := \Omega_X \times \Omega_Y \times \Omega_Z,$$

so that $\Omega = \Omega_{\text{space}}$ is a cubic domain with boundary $\partial\Omega$. The time interval is denoted by $I_T := [0, T]$, and the space-time domain is $\Omega_T := I_T \times \Omega_{\text{space}}$. We assume such a tensor-product structure for the computational domain in order to obtain a corresponding tensor structure for the matrices associated with the discrete operators, which will be advantageous for tensor-train (TT) approximations. A more detailed explanation of these tensor-network representations will be provided in Section 5.

In the remainder of this section we first introduce the space-time Chebyshev spectral collocation scheme (Section 2.1), then construct the staggered discrete spaces for \mathbf{E} and \mathbf{B} (Section 2.2), and finally describe the post-processing for recovering the magnetic field from the electric field (Section 2.3).

2.1. Space-time Chebyshev spectral collocation

We employ Chebyshev spectral collocation to discretize both spatial and temporal dimensions in the Maxwell equations. This space-time formulation allows us to solve for the electric field across all time steps simultaneously, enabling the tensor network compression techniques described in later sections.

We apply Chebyshev polynomials $T_k(x) = \cos(k \arccos(x))$ as global basis functions. The Chebyshev polynomials are particularly well-suited because they provide exponential convergence for smooth solutions while maintaining favorable conditioning properties. For computational convenience, we follow [11] and work with modified Chebyshev polynomials in each coordinate direction, including time.

For each coordinate $\xi \in \{t, x, y, z\}$ we denote by $\{\xi_i\}_{i=0}^{N_\xi}$ the Chebyshev–Gauss–Lobatto (CGL) collocation points [17] on $[-1, 1]$, and by $\{l_j^{(\xi)}\}_{j=0}^{N_\xi}$ the associated interpolating polynomials, which satisfy the property

$$l_j^{(\xi)}(\xi_i) = \begin{cases} 1 & \text{if } i = j, \\ 0 & \text{if } i \neq j, \end{cases}$$

for every coordinate $\xi \in \{t, x, y, z\}$. To lighten notation, we will often write $l_j(\xi)$ when the underlying coordinate is clear from the context.

This construction yields interpolating polynomials based on Chebyshev nodes, which provide the numerical advantages of Chebyshev polynomials while simplifying the implementation of boundary conditions and the evaluation of differential operators.

The one-dimensional CGL quadrature in a generic coordinate ξ provides exact integration for polynomials of degree up to $2N_\xi - 1$:

$$\int_{-1}^{+1} p(\xi) w(\xi) d\xi = \sum_{a=0}^{N_\xi} p(\xi_a) \omega_a, \quad w(\xi) = \frac{1}{\sqrt{1 - \xi^2}}, \quad (2.11)$$

where $\{\omega_a\}_{a=0}^{N_\xi}$ are the Chebyshev quadrature weights. After an affine mapping of each interval $\Omega_X, \Omega_Y, \Omega_Z, I_T$ to $[-1, 1]$, we use the same weight function w in each coordinate and define the weighted continuous L^2 -norm on the space–time domain $\Omega_T = I_T \times \Omega_{\text{space}}$ by

$$\|F\| := \left(\int_{\Omega_T} |F(t, \mathbf{x})|^2 w(t) w(x) w(y) w(z) dt dx \right)^{1/2}, \quad (2.12)$$

where $\mathbf{x} = (x, y, z)$.

Let $\{t_{a_4}\}_{a_4=0}^{N_t}, \{x_{a_1}\}_{a_1=0}^{N_x}, \{y_{a_2}\}_{a_2=0}^{N_y}$ and $\{z_{a_3}\}_{a_3=0}^{N_z}$ denote the CGL nodes in time and the three spatial directions, with corresponding quadrature weights $\{\omega_{a_4}^{(t)}\}, \{\omega_{a_1}^{(x)}\}, \{\omega_{a_2}^{(y)}\}$ and $\{\omega_{a_3}^{(z)}\}$. The associated discrete norm is

$$\|F\|_{N_t, N_x, N_y, N_z} := \left(\sum_{a_1=0}^{N_x} \sum_{a_2=0}^{N_y} \sum_{a_3=0}^{N_z} \sum_{a_4=0}^{N_t} |F(t_{a_4}, x_{a_1}, y_{a_2}, z_{a_3})|^2 \omega_{a_1}^{(x)} \omega_{a_2}^{(y)} \omega_{a_3}^{(z)} \omega_{a_4}^{(t)} \right)^{1/2}. \quad (2.13)$$

In what follows, we take the same polynomial degree in each coordinate, $N_t = N_x = N_y = N_z =: N$, and reuse the notation $\{\xi_a\}_{a=0}^N$ and $\{\omega_a\}_{a=0}^N$ for all coordinates. In that case we simply write

$$\|F\|_N := \left(\sum_{a_1, a_2, a_3, a_4=0}^N |F(t_{a_4}, x_{a_1}, y_{a_2}, z_{a_3})|^2 \omega_{a_1} \omega_{a_2} \omega_{a_3} \omega_{a_4} \right)^{1/2}. \quad (2.14)$$

For tensor-product polynomials of degree at most N in each coordinate, the discrete norm $\|\cdot\|_N$ is equivalent to the continuous norm $\|\cdot\|$. This ensures that the discrete and continuous problems have quantitatively comparable dynamics.

For later use, we also introduce the diagonal quadrature weight matrices on the one-dimensional collocation grids. Let $W_h \in \mathbb{R}^{(N+1) \times (N+1)}$ be the diagonal matrix whose entries are the Chebyshev weights $\{\omega_a\}_{a=0}^N$ from (2.14). Given a matrix $M \in \mathbb{R}^{(N+1) \times (N+1)}$ associated with a one-dimensional collocation grid, we denote by $\langle M \rangle$ the submatrix obtained by removing the first and last rows and columns, that is, the restriction of M to the $N - 1$ interior collocation points. Similarly, for matrices acting on the three-dimensional spatial grid we write $\langle\langle M \rangle\rangle$ for the restriction to interior spatial nodes. (The same notation will be used later for derivative and Laplacian matrices in Section 3.)

With this convention, the tensor-product weight matrix on the interior of the space–time grid is

$$W := \langle\langle W_h \rangle\rangle \otimes \langle\langle W_h \rangle\rangle \otimes \langle\langle W_h \rangle\rangle \otimes \langle W_h \rangle. \quad (2.15)$$

The matrix W defines the weighted ℓ^2 -norm $\|W^{1/2} \theta_h\|_2$ on vectors of interior space–time degrees of freedom, which will be used in the condition-number and convergence analysis of Section 4.

With the collocation grids, quadrature rules and norms in place, we now specify how the Maxwell unknowns are represented in these bases. Each component of the electric and magnetic fields is approximated by its tensor-product interpolant in the corresponding Chebyshev–Gauss–Lobatto nodes, expanded in the interpolating polynomials introduced above.

Expanding in terms of l_j 's, the discrete electric and magnetic fields can be written as

$$\begin{aligned}\mathbf{E}_h(t, \mathbf{x}) &= (E_{xh}, E_{yh}, E_{zh}) := \left(\sum_{j=0}^{N_{E_x}} E_x^j l_j^{E_x}(t, \mathbf{x}), \sum_{j=0}^{N_{E_y}} E_y^j l_j^{E_y}(t, \mathbf{x}), \sum_{j=0}^{N_{E_z}} E_z^j l_j^{E_z}(t, \mathbf{x}) \right), \\ \mathbf{B}_h(t, \mathbf{x}) &= (B_{xh}, B_{yh}, B_{zh}) := \left(\sum_{j=0}^{N_{B_x}} B_x^j l_j^{B_x}(t, \mathbf{x}), \sum_{j=0}^{N_{B_y}} B_y^j l_j^{B_y}(t, \mathbf{x}), \sum_{j=0}^{N_{B_z}} B_z^j l_j^{B_z}(t, \mathbf{x}) \right),\end{aligned}\quad (2.16)$$

where $\mathbf{x} = (x, y, z)$ and the superscript on l_j indicates the field component with which the basis functions and associated collocation grid are aligned. The integers $N_{E_i} + 1$ and $N_{B_i} + 1$ denote the number of spatial degrees of freedom used for each component E_i and B_i , respectively. These numbers differ between components due to the staggered grid construction described in Section 2.2. This ensures proper coupling between electric and magnetic field components through the discrete curl operator. We now construct discrete differential operators acting on these expansions.

The core of the spectral collocation method lies in constructing matrix representations of differential operators. We build all spatial and temporal operators from the fundamental one-dimensional derivative matrices. For the x -direction we define

$$(\mathbf{S}_x)_{ij} := \frac{d}{dx} l_j^{(x)}(x) \Big|_{x=x_i}, \quad (2.17)$$

and analogously obtain \mathbf{S}_y , \mathbf{S}_z and \mathbf{S}_t in the y -, z -, and t -directions. We construct the first-order derivative matrix \mathbf{S}_x of size $(N_x+1) \times (N_x+1)$ (and similarly for the other directions). Second-order derivative matrices are obtained through matrix multiplication of the first-order derivatives:

$$(\mathbf{S}_{xx})_{ij} = \sum_{s=0}^{N_x} (\mathbf{S}_x)_{is} (\mathbf{S}_x)_{sj}. \quad (2.18)$$

A complete derivation for this expression can be found in [11].

To construct operators acting on the full four-dimensional space–time domain $\Omega_T = I_T \times \Omega_{\text{space}}$, we use Kronecker products of the one-dimensional operators. The Laplacian operator becomes

$$\mathbf{A}_\Delta = \mathbf{I}_t \otimes \mathbf{S}_{xx} \otimes \mathbf{I}_y \otimes \mathbf{I}_z + \mathbf{I}_t \otimes \mathbf{I}_x \otimes \mathbf{S}_{yy} \otimes \mathbf{I}_z + \mathbf{I}_t \otimes \mathbf{I}_x \otimes \mathbf{I}_y \otimes \mathbf{S}_{zz}, \quad (2.19)$$

where \mathbf{I}_ξ denotes the identity matrix of appropriate size for coordinate $\xi \in \{x, y, z, t\}$.

The curl operator components are constructed using spatial derivatives only:

$$\nabla \times \mathbf{v} = \left(\frac{\partial v_z}{\partial y} - \frac{\partial v_y}{\partial z}, \frac{\partial v_x}{\partial z} - \frac{\partial v_z}{\partial x}, \frac{\partial v_y}{\partial x} - \frac{\partial v_x}{\partial y} \right), \quad (2.20)$$

where the associated matrix operators are

$$\begin{aligned}\mathbf{D}_x &:= \mathbf{I}_t \otimes \mathbf{S}_x \otimes \mathbf{I}_y \otimes \mathbf{I}_z, & \mathbf{D}_y &:= \mathbf{I}_t \otimes \mathbf{I}_x \otimes \mathbf{S}_y \otimes \mathbf{I}_z, \\ \mathbf{D}_z &:= \mathbf{I}_t \otimes \mathbf{I}_x \otimes \mathbf{I}_y \otimes \mathbf{S}_z, & \mathbf{D}_t &:= \mathbf{S}_t \otimes \mathbf{I}_x \otimes \mathbf{I}_y \otimes \mathbf{I}_z.\end{aligned}\quad (2.21)$$

The matrices corresponding to the curl operator components are constructed as linear combinations of \mathbf{D}_x , \mathbf{D}_y , and \mathbf{D}_z , while \mathbf{D}_t represents the temporal derivative operator and will be used in the reconstruction of the magnetic field.

2.2. Staggered space-time discrete spaces

To preserve the divergence-free property of the magnetic field, $\nabla \cdot \mathbf{B} = 0$, in our discretization, we introduce a staggered spectral collocation approach within the space-time framework developed in Section 2.1.

In classical finite-difference staggered grids, different field components are evaluated at spatially shifted locations to improve stability and enforce discrete conservation laws. In our spectral method, we achieve analogous staggering not through spatial shifts, but by using *different polynomial degrees* for electric and magnetic field components in different coordinate directions.

Specifically, we collocate the electric field components \mathbf{E} at Chebyshev–Gauss–Lobatto (CGL) nodes, which correspond to polynomials of a certain degree, while magnetic field components \mathbf{B} are collocated at Chebyshev–Gauss (CG) nodes—the interior points that exclude the boundaries. This spectral staggering maintains exponential convergence while inheriting the stability and conservation properties of classical staggered grids.

The key insight is that the discrete curl operator $\nabla_h \times \mathbf{E}_h$, assembled from the one-dimensional derivative matrices in (2.21), must map between compatible discrete spaces. By carefully constructing polynomial spaces with different degrees of freedom for each field component, we ensure that:

1. The discrete curl accurately approximates $\partial \mathbf{B}_h / \partial t$ at each time step
2. The discrete identity $\nabla \cdot (\nabla \times \cdot) = 0$ holds to spectral accuracy
3. The constraint $\nabla_h \cdot \mathbf{B}_h \approx 0$ is maintained throughout the computation

Unlike finite-difference methods where staggering involves pointwise evaluations at shifted spatial locations, our spectral staggered grid uses different polynomial degrees for electric and magnetic field components in different coordinate directions [29, 16]. This approach preserves spectral accuracy while providing the structural benefits of classical staggering.

Recall that the one-dimensional computational domains in each spatial direction are intervals $\Omega_X, \Omega_Y, \Omega_Z \subset \mathbb{R}$ and that the time interval is $I_T = [0, T]$, so that $\Omega_{\text{space}} = \Omega_X \times \Omega_Y \times \Omega_Z$ and $\Omega_T = I_T \times \Omega_{\text{space}}$. Under the constant-coefficient assumptions stated in Section 2, the Maxwell system reduces to the vector wave equation (2.6) for the electric field. The design of the discrete spaces is crucial to ensure that the discrete curl and divergence operators satisfy the same structural relations as in the continuous case.

The key insight is that the discrete curl operator $\nabla_h \times \mathbf{E}_h$, assembled from the one-dimensional derivative matrices in (2.21), must accurately approximate $\partial \mathbf{B}_h / \partial t$ at each time step and map between compatible discrete spaces. This requires a careful construction of polynomial spaces with different degrees of freedom for each field component, so that the discrete analogue of the identity $\nabla \cdot (\nabla \times \cdot) = 0$ holds asymptotically and the constraint $\nabla_h \cdot \mathbf{B}_h \approx 0$ is maintained.

Let $\mathbb{P}_k(I)$ denote the space of polynomials of degree at most k on an interval I . We construct distinct tensor-product polynomial spaces for each component of the magnetic field $\mathbf{B} = (B_x, B_y, B_z)$:

$$\begin{aligned} S_k^x &:= \mathbb{P}_{k+1}(I_T) \otimes \mathbb{P}_{k+1}(\Omega_X) \otimes \mathbb{P}_k(\Omega_Y) \otimes \mathbb{P}_k(\Omega_Z), \\ S_k^y &:= \mathbb{P}_{k+1}(I_T) \otimes \mathbb{P}_k(\Omega_X) \otimes \mathbb{P}_{k+1}(\Omega_Y) \otimes \mathbb{P}_k(\Omega_Z), \\ S_k^z &:= \mathbb{P}_{k+1}(I_T) \otimes \mathbb{P}_k(\Omega_X) \otimes \mathbb{P}_k(\Omega_Y) \otimes \mathbb{P}_{k+1}(\Omega_Z). \end{aligned} \quad (2.22)$$

For the magnetic field component B_i , we use polynomials of degree $k+1$ in the temporal direction and in the corresponding i -th spatial direction, and polynomials of degree k in the remaining two spatial directions. In practice, this means B_x is collocated at $(N+1) \times (N+1) \times N \times N$ points in the (t, x, y, z) directions, while E_x is collocated at $(N+1) \times N \times (N+1) \times (N+1)$ points, where $N = k+1$.

For the electric field components $\mathbf{E} = (E_x, E_y, E_z)$, we define complementary spaces:

$$\begin{aligned} V_k^x &:= \mathbb{P}_{k+1}(I_T) \otimes \mathbb{P}_k(\Omega_X) \otimes \mathbb{P}_{k+1}(\Omega_Y) \otimes \mathbb{P}_{k+1}(\Omega_Z), \\ V_k^y &:= \mathbb{P}_{k+1}(I_T) \otimes \mathbb{P}_{k+1}(\Omega_X) \otimes \mathbb{P}_k(\Omega_Y) \otimes \mathbb{P}_{k+1}(\Omega_Z), \\ V_k^z &:= \mathbb{P}_{k+1}(I_T) \otimes \mathbb{P}_{k+1}(\Omega_X) \otimes \mathbb{P}_{k+1}(\Omega_Y) \otimes \mathbb{P}_k(\Omega_Z). \end{aligned} \quad (2.23)$$

Here, the electric field component E_i uses degree k in the i -th spatial direction and degree $k+1$ in the other two spatial directions, while being of degree $k+1$ in time. This choice is complementary to the construction of the magnetic-field spaces in (2.22).

This staggered construction ensures that when we compute

$$\frac{\partial \mathbf{B}_h}{\partial t} = -\nabla_h \times \mathbf{E}_h$$

using the discrete curl operator built from $\mathbf{D}_x, \mathbf{D}_y, \mathbf{D}_z$ in (2.21), the resulting magnetic-field components naturally lie in the spaces S_k^i and satisfy the discrete divergence-free constraint to high accuracy. In particular, the curl operation maps from the electric field spaces V_k^i to the magnetic field spaces S_k^i while preserving spectral accuracy and maintaining the proper relationships between degrees of freedom.

The choice of which components use degree k versus $k+1$ in each direction is dictated by the structure of Maxwell's curl equations—ensuring that when we differentiate a degree $k+1$ polynomial, we obtain a degree k polynomial that naturally lives in the correct discrete space. We now collect the component-wise spaces into vector-valued discrete spaces for the magnetic and electric fields:

$$\begin{aligned} \mathcal{S}_h &:= S_k^x \times S_k^y \times S_k^z \quad (\text{for the magnetic field } \mathbf{B}_h), \\ \mathcal{V}_h &:= V_k^x \times V_k^y \times V_k^z \quad (\text{for the electric field } \mathbf{E}_h). \end{aligned} \quad (2.24)$$

Thus, each component B_i (respectively, E_i) belongs to S_k^i (respectively, V_k^i), and the expansions in (2.16) are consistent with these spaces and the associated staggered collocation grids.

At the level of the wave equation, the fully discrete space–time scheme for the electric field can be written formally as: find $\mathbf{E}_h \in \mathcal{V}_h$ such that

$$\frac{\partial^2 \mathbf{E}_h}{\partial t^2} - c^2 \Delta \mathbf{E}_h = -c^2 \nabla \rho_h - \frac{1}{\epsilon_0} \frac{d \mathbf{J}_h}{dt}, \quad (2.25)$$

where ρ_h and \mathbf{J}_h denote the interpolants of the charge and current densities onto the collocation grid, and the differential operators are discretized using the matrices introduced in Section 2.1 (e.g. the Laplacian matrix \mathbf{A}_Δ in (2.19) and the first-order derivative matrices in (2.21)). The explicit matrix form of (2.25), including the Kronecker structure of the resulting operator, will be derived in Section 3.

The different degrees of freedom for each component in the staggered spaces \mathcal{S}_h and \mathcal{V}_h require a dedicated post-processing step to recover the magnetic field from the electric field solution. This post-processing, based on the discrete Faraday law, is outlined in Section 2.3 and later revisited in matrix form in Section 3.1.

2.3. Post-processing to recover the magnetic field

Our space–time spectral discretization solves the wave equation for the electric field and computes a space–time approximation $\mathbf{E}_h \in \mathcal{V}_h$ across all collocation points (see Sections 2.1 and 2.2).

The magnetic field $\mathbf{B}_h \in \mathcal{S}_h$ is then obtained in a separate, but fully consistent, post-processing step based on the discrete version of Faraday's law:

$$\frac{\partial \mathbf{B}_h}{\partial t} = -\nabla_h \times \mathbf{E}_h. \quad (2.26)$$

Here $\nabla_h \times$ denotes the discrete curl operator assembled from the one-dimensional derivative matrices introduced in (2.21). This equation is evaluated entirely within the tensor-product spectral framework described in Sections 2.1–2.2.

We view the discrete electric field \mathbf{E}_h given by the space–time solve in its interpolant form based on the CGL nodes. Each component of the electric field can be written as

$$E_{ih}(t, \mathbf{x}) = \sum_{a_1, a_2, a_3, a_4=0}^N E_i^{a_1, a_2, a_3, a_4} l_{a_1}^{E_i}(x) l_{a_2}^{E_i}(y) l_{a_3}^{E_i}(z) l_{a_4}^{E_i}(t), \quad i \in \{x, y, z\}, \quad (2.27)$$

where $\mathbf{x} = (x, y, z)$, the functions $l_{a_j}^{E_i}$ are the component-wise basis functions associated with the staggered collocation grids, and $E_i^{a_1, a_2, a_3, a_4}$ are the coefficients obtained from the space–time solve in \mathcal{V}_h . This expression particularly is very useful to derive the low-rank structure of the associated matrices.

To compute the magnetic field from (2.26), we apply the discrete curl operator built from the matrices in (2.21) to the interpolant (2.27). By construction of the staggered spaces in Section 2.2, the electric field lives in \mathcal{V}_h and the discrete curl $\nabla_h \times$ maps from \mathcal{V}_h into \mathcal{S}_h . Consequently, the reconstructed magnetic field \mathbf{B}_h automatically belongs to the correct discrete space and remains compatible with the electric field representation. This staggered mapping preserves the discrete divergence-free condition $\nabla_h \cdot \mathbf{B}_h \approx 0$ and maintains the overall spectral accuracy of the scheme.

The discussion in this section is intentionally kept at a conceptual level. In Section 3.1, we revisit the magnetic field recovery and derive the corresponding matrix equations in detail, highlighting the Kronecker and tensor-train structure of the post-processing step.

3. Wave equation in the space–time spectral collocation scheme

In Sections 2.1–2.3, we introduced the space–time Chebyshev spectral collocation framework and the staggered spaces \mathcal{V}_h and \mathcal{S}_h for the electric and magnetic fields, respectively. Under the constant-coefficient assumptions in Section 2, the Maxwell system reduces to the vector wave equation (2.6) for the electric field. In this section, we derive the explicit space–time matrix formulation of this wave equation for a single component of the electric field. This will reveal the Kronecker structure of the discrete operator and motivate the low-rank tensor representations exploited in later sections.

For notational convenience we abbreviate the spatial domain by $\Omega := \Omega_{\text{space}}$, so that $\Omega_T = I_T \times \Omega$. We detail the derivation for the x -component of the electric field; the y - and z -components are treated analogously and lead to systems of the same form.

We begin by rewriting the wave equation (2.7) in first-order form and then present its discretization using the space–time spectral collocation method introduced in Section 2.1. The resulting system naturally admits a low-rank tensor representation, which will be exploited in later sections.

Let us define the auxiliary variable for the x -component of the electric field as

$$\mathbf{v} = \begin{bmatrix} v \\ v_t \end{bmatrix} := \begin{bmatrix} E_x \\ \frac{\partial E_x}{\partial t} \end{bmatrix},$$

and define the corresponding source term as

$$f := -c^2 \frac{\partial \rho}{\partial x} - \frac{1}{\epsilon_0} \frac{dJ_x}{dt}.$$

Then, the second-order wave equation can be written as the first-order system

$$\frac{d\mathbf{v}}{dt} = \begin{bmatrix} 0 & I \\ c^2 \Delta & 0 \end{bmatrix} \mathbf{v} + \begin{bmatrix} 0 \\ f \end{bmatrix}, \quad (3.1)$$

with boundary and initial conditions

$$\mathbf{v}(t, \partial\Omega) = \begin{bmatrix} v^{\text{bd}}(t, \mathbf{x}) \\ v_t^{\text{bd}}(t, \mathbf{x}) \end{bmatrix}, \quad \mathbf{v}(0, \Omega) = \begin{bmatrix} v^0(\mathbf{x}) \\ v_t^0(\mathbf{x}) \end{bmatrix},$$

where v^{bd} and v_t^{bd} prescribe boundary data for E_x and its time derivative on $\partial\Omega$, while v^0 and v_t^0 denote the initial value and the initial time derivative of E_x at $t = 0$.

Let \mathbf{v}_h denote the values of \mathbf{v} evaluated at the space-time collocation grid. The discretized form of (3.1) becomes

$$\begin{bmatrix} \mathbf{S}_t \otimes \mathbf{I}_{(N+1)^3} & \mathbf{0} \\ \mathbf{0} & \mathbf{S}_t \otimes \mathbf{I}_{(N+1)^3} \end{bmatrix} \begin{bmatrix} \mathbf{v}_h \\ \mathbf{v}_{th} \end{bmatrix} = \begin{bmatrix} \mathbf{0} & \mathbf{I}_{N+1} \otimes \mathbf{I}_{(N+1)^3} \\ \mathbf{I}_{N+1} \otimes \mathbf{A}_\Delta & \mathbf{0} \end{bmatrix} \begin{bmatrix} \mathbf{v}_h \\ \mathbf{v}_{th} \end{bmatrix} + \begin{bmatrix} \mathbf{0} \\ \mathbf{f}_h \end{bmatrix}, \quad (3.2)$$

where \mathbf{f}_h is the discretized source, and \mathbf{I}_m denotes the $m \times m$ identity matrix. The matrix \mathbf{A}_Δ is the discrete Laplacian defined in (2.19).

We next eliminate the known boundary and initial conditions and restrict the system to interior space-time points. Let $\hat{\mathbf{v}}_h$ and $\hat{\mathbf{v}}_{th}$ denote the unknown interior values of E_x and its time derivative. Denoting by $\langle \mathbf{S}_t \rangle$ and $\langle \langle \mathbf{A}_\Delta \rangle \rangle$ the restrictions of \mathbf{S}_t and \mathbf{A}_Δ to interior time and space nodes, respectively, we obtain

$$\begin{bmatrix} \langle \mathbf{S}_t \rangle \otimes \mathbf{I}_{(N-1)^3} & \mathbf{0} \\ \mathbf{0} & \langle \mathbf{S}_t \rangle \otimes \mathbf{I}_{(N-1)^3} \end{bmatrix} \begin{bmatrix} \hat{\mathbf{v}}_h \\ \hat{\mathbf{v}}_{th} \end{bmatrix} = \begin{bmatrix} \mathbf{0} & \mathbf{I}_N \otimes \mathbf{I}_{(N-1)^3} \\ \mathbf{I}_N \otimes \langle \langle \mathbf{A}_\Delta \rangle \rangle & \mathbf{0} \end{bmatrix} \begin{bmatrix} \hat{\mathbf{v}}_h \\ \hat{\mathbf{v}}_{th} \end{bmatrix} + \begin{bmatrix} \mathbf{0} \\ \hat{\mathbf{f}}_h \end{bmatrix} - \begin{bmatrix} \mathbf{A}_t \mathbf{v}_h^0 \\ \mathbf{A}_t \mathbf{v}_{th}^0 \end{bmatrix} + \begin{bmatrix} \mathbf{G} \mathbf{v}_h^{\text{bd}} \\ \mathbf{G}_t \mathbf{v}_{th}^{\text{bd}} \end{bmatrix}, \quad (3.3)$$

where

$$\begin{aligned} \mathbf{A}_t &:= \mathbf{S}_t(I_t^{\text{int}}, :) \otimes \mathbf{I}_z(I_z^{\text{int}}, :) \otimes \mathbf{I}_y(I_y^{\text{int}}, :) \otimes \mathbf{I}_x(I_x^{\text{int}}, :), \\ \mathbf{G} &:= \mathbf{I}_t(I_t^{\text{int}}, :) \otimes \mathbf{I}_z(I_z^{\text{int}}, :) \otimes \mathbf{I}_y(I_y^{\text{int}}, :) \otimes \mathbf{I}_x(I_x^{\text{int}}, :), \\ \mathbf{G}_t &:= \mathbf{I}_t(I_t^{\text{int}}, :) \otimes \mathbf{I}_z(I_z^{\text{int}}, :) \otimes \mathbf{I}_y(I_y^{\text{int}}, :) \otimes \mathbf{S}_{xx}(I_x^{\text{int}}, :) \\ &\quad + \mathbf{I}_t(I_t^{\text{int}}, :) \otimes \mathbf{I}_z(I_z^{\text{int}}, :) \otimes \mathbf{S}_{yy}(I_y^{\text{int}}, :) \otimes \mathbf{I}_x(I_x^{\text{int}}, :) \\ &\quad + \mathbf{I}_t(I_t^{\text{int}}, :) \otimes \mathbf{S}_{zz}(I_z^{\text{int}}, :) \otimes \mathbf{I}_y(I_y^{\text{int}}, :) \otimes \mathbf{I}_x(I_x^{\text{int}}, :). \end{aligned} \quad (3.4)$$

Here, for a matrix \mathbf{M} and an index set I , the notation $\mathbf{M}(I, :)$ denotes the submatrix consisting of rows indexed by I . The sets $I_t^{\text{int}}, I_x^{\text{int}}, I_y^{\text{int}}, I_z^{\text{int}}$ collect the indices of interior nodes in time and in each spatial direction, respectively. The boundary data is stored in the vectors \mathbf{v}_h^{bd} and $\mathbf{v}_{th}^{\text{bd}}$ (discrete counterparts of v^{bd} and v_t^{bd}), initial data in vectors \mathbf{v}_h^0 and \mathbf{v}_{th}^0 (discrete counterparts of v^0 and v_t^0), and $\hat{\mathbf{f}}_h$ denotes the interior part of the source after boundary elimination.

Decoupling (3.3) we get:

$$\hat{\mathbf{v}}_{th} = (\langle \mathbf{S}_t \rangle \otimes \mathbf{I}_{(N-1)^3}) \hat{\mathbf{v}}_h + \mathbf{A}_t \mathbf{v}_h^0 - \mathbf{G} \mathbf{v}_h^{\text{bd}}, \quad (3.5)$$

from the first block and the following in the second block

$$(\mathbf{I}_N \otimes \langle\langle \mathbf{A}_\Delta \rangle\rangle) \hat{\mathbf{v}}_h = (\langle\langle \mathbf{S}_t \rangle\rangle \otimes \mathbf{I}_{(N-1)^3}) \hat{\mathbf{v}}_{th} - \hat{\mathbf{f}}_h + \mathbf{A}_t \mathbf{v}_{th}^0 - \mathbf{G}_t \mathbf{v}_{th}^{\text{bd}}. \quad (3.6)$$

Eliminating $\hat{\mathbf{v}}_{th}$, we get a system in terms of $\hat{\mathbf{v}}_h$:

$$\mathbf{A}_{Lap} \hat{\mathbf{v}}_h = \mathbf{F} - \mathbf{F}^{\text{BD}}, \quad (3.7)$$

with

$$\begin{aligned} \mathbf{A}_{Lap} &:= (\langle\langle \mathbf{S}_t \rangle\rangle^2 \otimes \mathbf{I}_{(N-1)^3}) - (\mathbf{I}_N \otimes \langle\langle \mathbf{A}_\Delta \rangle\rangle), \\ \mathbf{F} &= \hat{\mathbf{f}}_h, \\ \mathbf{F}^{\text{BD}} &= \mathbf{A}_t \mathbf{v}_{th}^0 - \mathbf{G}_t \mathbf{v}_{th}^{\text{bd}} + (\langle\langle \mathbf{S}_t \rangle\rangle \otimes \mathbf{I}_{(N-1)^3}) \mathbf{A}_t \mathbf{v}_h^0 - (\langle\langle \mathbf{S}_t \rangle\rangle \otimes \mathbf{I}_{(N-1)^3}) \mathbf{G} \mathbf{v}_h^{\text{bd}}, \end{aligned}$$

where \mathbf{F}^{BD} collects all the discrete initial and boundary contributions. Thus, the fully discrete space-time wave equation for the x -component reduces to the linear system (3.7). The same discretization procedure applies to the y - and z -components of the electric field. Replacing E_x by E_y or E_z , and J_x by J_y or J_z , respectively, leads to systems of the form (3.7) for each spatial direction. The tensor structure and solution strategy remain identical.

The operator \mathbf{A}_{Lap} in (3.7) is assembled using Kronecker products of one-dimensional matrices in time and each spatial dimension. This structure is ideal for approximation in TT format, enabling scalable algorithms in higher dimensions.

3.1. Recovering the magnetic field

Once the electric field components $\mathbf{E}_h = (\mathbf{E}_{xh}, \mathbf{E}_{yh}, \mathbf{E}_{zh}) \in \mathcal{V}_h$ have been computed from the space-time wave equation (3.7), we recover the magnetic field $\mathbf{B}_h = (\mathbf{B}_{xh}, \mathbf{B}_{yh}, \mathbf{B}_{zh}) \in \mathcal{S}_h$ using the discrete version of Faraday's law, as previewed in Section 2.3. The discrete magnetic field components are governed by the system

$$\begin{aligned} \frac{\partial B_{xh}}{\partial t} &= -\underbrace{\frac{\partial E_{zh}}{\partial y} + \frac{\partial E_{yh}}{\partial z}}_{=: H_{xh}}, \\ \frac{\partial B_{yh}}{\partial t} &= +\underbrace{\frac{\partial E_{zh}}{\partial x} - \frac{\partial E_{xh}}{\partial z}}_{=: H_{yh}}, \\ \frac{\partial B_{zh}}{\partial t} &= -\underbrace{\frac{\partial E_{yh}}{\partial x} + \frac{\partial E_{xh}}{\partial y}}_{=: H_{zh}}. \end{aligned} \quad (3.8)$$

Here H_{ih} represent the curl components of the electric field. Using the matrix operators defined in (2.21), each magnetic field component satisfies a linear system of the form

$$\mathbf{D}_t \mathbf{B}_{ih} = \mathbf{H}_{ih}, \quad i \in \{x, y, z\}, \quad (3.9)$$

where $\mathbf{D}_t := \mathbf{S}_t \otimes \mathbf{I}_x \otimes \mathbf{I}_y \otimes \mathbf{I}_z$ is the temporal derivative operator and $\mathbf{B}_{ih}, \mathbf{H}_{ih}$ denote the vectors of collocation values of B_{ih} and H_{ih} .

For the x -component of the magnetic field, the right-hand side \mathbf{H}_{xh} is computed using the spatial derivative operators:

$$\mathbf{H}_{xh} = -(\mathbf{I}_t \otimes \mathbf{I}_x \otimes \mathbf{S}_y \otimes \mathbf{I}_z) \mathbf{E}_{zh} + (\mathbf{I}_t \otimes \mathbf{I}_x \otimes \mathbf{I}_y \otimes \mathbf{S}_z) \mathbf{E}_{yh}. \quad (3.10)$$

Due to the staggered grid construction described in Section 2.2, the electric field components E_{yh} and E_{zh} belong to the spaces S_k^y and S_k^z , respectively, while the magnetic field component B_{xh} belongs to the space V_k^x . The interpolation between these spaces is handled through projection matrices that preserve spectral accuracy.

After applying boundary conditions, the system (3.9) for interior nodes becomes

$$\mathbf{A}_{\text{curl}} \hat{\mathbf{B}}_{xh} = \mathbf{F}_{\text{curl}} - \mathbf{F}_{\text{curl}}^{\text{BD}}, \quad (3.11)$$

where

$$\mathbf{A}_{\text{curl}} := \langle \mathbf{S}_t \rangle \otimes \mathbf{I}_x^{\text{int}} \otimes \mathbf{I}_y^{\text{int}} \otimes \mathbf{I}_z^{\text{int}}, \quad (3.12)$$

$$\mathbf{F}_{\text{curl}} := \hat{\mathbf{H}}_{xh}, \quad (3.13)$$

$$\mathbf{F}_{\text{curl}}^{\text{BD}} := \mathbf{D}_t^{\text{int}} \mathbf{B}_{xh}^{\text{bd}}. \quad (3.14)$$

In these expressions, the superscript int denotes restriction to interior collocation points. For each spatial coordinate $\xi \in \{x, y, z\}$ we denote by I_ξ^{int} the index set of interior nodes in that direction, and we define the corresponding interior identity matrices as

$$\mathbf{I}_\xi^{\text{int}} := \mathbf{I}_\xi(I_\xi^{\text{int}}, I_\xi^{\text{int}}), \quad \xi \in \{x, y, z\}.$$

Similarly, the temporal–spatial derivative operator restricted to the interior is defined by

$$\mathbf{D}_t^{\text{int}} := \mathbf{S}_t(I_t^{\text{int}}, :) \otimes \mathbf{I}_x(I_x^{\text{int}}, :) \otimes \mathbf{I}_y(I_y^{\text{int}}, :) \otimes \mathbf{I}_z(I_z^{\text{int}}, :).$$

The vector $\mathbf{B}_{xh}^{\text{bd}}$ contains the boundary values of B_{xh} , and boldface symbols such as \mathbf{B}_{xh} and \mathbf{F}_{curl} represent vectors of discrete collocation values rather than continuous fields.

The curl computation in (3.13) requires interpolation between different staggered spaces. Specifically, we have

$$\begin{aligned} \mathbf{F}_{\text{curl}} = & -(\mathbf{I}_t^{\text{int}} \otimes \mathbf{I}_x^{\text{int}} \otimes \langle \langle \mathbf{S}_y \rangle \rangle \otimes \mathbf{I}_z^{\text{int}}) \mathcal{I}_{V_z \rightarrow S_x} \hat{\mathbf{E}}_{zh} \\ & + (\mathbf{I}_t^{\text{int}} \otimes \mathbf{I}_x^{\text{int}} \otimes \mathbf{I}_y^{\text{int}} \otimes \langle \langle \mathbf{S}_z \rangle \rangle) \mathcal{I}_{V_y \rightarrow S_x} \hat{\mathbf{E}}_{yh}, \end{aligned} \quad (3.15)$$

where $\mathcal{I}_{V_z \rightarrow S_x}$ and $\mathcal{I}_{V_y \rightarrow S_x}$ represent interpolation operators mapping from electric-field spaces V_k^z and V_k^y to the magnetic-field space S_k^x . The magnetic field recovery for components B_{yh} and B_{zh} follows the same pattern as described above for B_{xh} , with appropriate modifications to the spatial derivative operators and interpolation matrices according to the staggered grid construction in (2.22)–(2.23).

This post-processing approach ensures that the reconstructed magnetic field \mathbf{B}_h maintains the same spectral accuracy as the electric field solution, preserves the discrete divergence-free constraint $\nabla_h \cdot \mathbf{B}_h \approx 0$, and maintains the tensor-product structure required for efficient implementation in tensor-train format.

4. Condition number estimates and spectral convergence

In this section we study two complementary analytical properties of the proposed space–time spectral collocation scheme. First, we derive condition number estimates for the discrete operators arising in the wave equation formulation and in the magnetic-field reconstruction, namely the matrices \mathbf{A}_{Lap} and \mathbf{A}_{curl} introduced in Sections 3 and 3.1. These estimates quantify the stability of the discrete systems and are relevant for the performance of iterative solvers and tensor-train approximations. Second, we establish spectral convergence of the discrete electric and magnetic fields, as well as exponential decay of the discrete divergence errors associated with Gauss’s laws.

4.1. Condition number estimates

We recall the spectral condition number of a matrix \mathbf{M} , defined by

$$\kappa(\mathbf{M}) := \frac{\max_{\lambda \in \Lambda(\mathbf{M})} |\lambda|}{\min_{\lambda \in \Lambda(\mathbf{M})} |\lambda|}, \quad (4.1)$$

where $\Lambda(\mathbf{M})$ denotes the spectrum of \mathbf{M} . Throughout this subsection, for a complex number z we write $Re(z)$ and $Im(z)$ for the real and imaginary parts of z , respectively.

We collect several lemmas that describe the spectral properties of Chebyshev derivative matrices [24]. Here \mathbf{S} denotes a generic one-dimensional Chebyshev first-derivative matrix (in any of the variables t, x, y, z), and $\langle \mathbf{S} \rangle$, $\langle \langle \mathbf{S}^2 \rangle \rangle$ denote the corresponding restrictions to interior nodes, as in Section 3.

Lemma 4.1. *Let $N \geq 1$, and $\lambda \in \Lambda(\langle \mathbf{S} \rangle)$. Then*

$$Re(\lambda) \geq CN,$$

where C is a positive constant independent of N .

Lemma 4.2. *Let $N \geq 1$, and $\lambda \in \Lambda(\langle \mathbf{S} \rangle)$. Then*

$$|\lambda| \leq cN^2,$$

where c is a positive constant independent of N .

Lemma 4.3. *Let $N \geq 2$. Then the eigenvalues of $-\langle \langle \mathbf{S}^2 \rangle \rangle$ are real, bounded below by c and above by CN^4 , where c and C are positive constants independent of N .*

Theorem 4.1. *Let $N \geq 2$, and let \mathbf{A}_{Lap} be the Chebyshev spectral collocation matrix defined in (3.7), and λ be any eigenvalue of \mathbf{A}_{Lap} . Then*

$$c \leq |\lambda| \leq CN^4. \quad (4.2)$$

Consequently,

$$\kappa(\mathbf{A}_{Lap}) \leq CN^4. \quad (4.3)$$

Proof. Let $\lambda \in \Lambda(\mathbf{A}_{Lap})$, where $\Lambda(\mathbf{A}_{Lap})$ denotes the spectrum of \mathbf{A}_{Lap} . Then we can write

$$\lambda = \gamma^2 + 3\mu, \quad (4.4)$$

where $\gamma = Re(\gamma) + i Im(\gamma)$ is an eigenvalue of $\langle \mathbf{S}_t \rangle$, and μ is an eigenvalue of $-\langle \langle \mathbf{S}_\nu^2 \rangle \rangle$, with $\nu \in \{x, y, z\}$. A straightforward calculation yields

$$\begin{aligned} |\lambda|^2 &= Re(\gamma)^4 + 6\mu Re(\gamma)^2 + 2Re(\gamma)^2 Im(\gamma)^2 + (3\mu - Im(\gamma))^2 \\ &\geq Re(\gamma)^4 + 6\mu Re(\gamma)^2 \geq c, \end{aligned} \quad (4.5)$$

using Lemma 4.1 and Lemma 4.3. Moreover, by Lemma 4.2 we obtain

$$|\lambda|^2 \leq CN^8. \quad (4.6)$$

Hence $c \leq |\lambda| \leq CN^4$, and therefore $\kappa(\mathbf{A}_{Lap}) \leq CN^4$. \square

We now focus on the spectrum of the matrix associated with the magnetic-field reconstruction defined in (3.11).

Theorem 4.2. Let $N \geq 1$, and let \mathbf{A}_{curl} be the Chebyshev spectral collocation matrix defined in (3.11), and λ be an eigenvalue of \mathbf{A}_{curl} . Then

$$c \leq |\lambda| \leq CN^2, \quad (4.7)$$

and

$$\kappa(\mathbf{A}_{\text{curl}}) \leq CN^2, \quad (4.8)$$

where C is a positive generic constant independent of N .

Proof. The result follows directly from Lemma 4.1 and Lemma 4.2, applied to the temporal derivative matrix appearing in \mathbf{A}_{curl} . \square

4.2. Spectral convergence

We now discuss the spectral convergence of the fully discrete scheme for both the wave equation and the Maxwell system. The first result concerns the componentwise wave equation for the electric field; the second addresses the magnetic field obtained via post-processing; and the third quantifies the convergence of the discrete Gauss law for \mathbf{E} and the discrete divergence-free constraint for \mathbf{B} .

Theorem 4.3. Let E_x be the solution of (2.7). Assume that E_x is an analytic function in t, x, y , and z . Let $N \geq 2$, and let \hat{v}_h be the solution of the space-time method defined in Section 3. Further, let Θ_h be the error associated with the collocation approximation \hat{v}_h of E_x . Then

$$|W^{1/2}\Theta_h|_2 \leq c N^{4.5} e^{-CN}, \quad (4.9)$$

where the weight matrix W is defined in (2.15), and $|\cdot|_2$ denotes vector/ matrix 2 norm.

Proof. We assume that Ω_h is the computational grid. Let N^{dof} be the total number of grid points, and $N_{\text{int}}^{\text{dof}}$ be the total number of interior points in space. Then, we can write $E_{xh}(t)$ as

$$E_{xh}(t) := \begin{bmatrix} E_x(t, \mathbf{x}_1) \\ E_x(t, \mathbf{x}_2) \\ \vdots \\ E_x(t, \mathbf{x}_{N_{\text{int}}^{\text{dof}}}) \end{bmatrix}_{N_{\text{int}}^{\text{dof}} \times 1},$$

and similarly

$$f_h(t) := \begin{bmatrix} f(t, \mathbf{x}_1) \\ f(t, \mathbf{x}_2) \\ \vdots \\ f(t, \mathbf{x}_{N_{\text{int}}^{\text{dof}}}) \end{bmatrix}_{N_{\text{int}}^{\text{dof}} \times 1}.$$

A semi-discrete approximation of the wave equation (2.7) is

$$\begin{aligned} \frac{d^2 E_{xh}(t)}{dt^2} &= \sum_{j=2}^N \left(\mathbf{A} E_{xh}(t_j) + f_h(t_j) \right) l_j(t), \\ E_{xh}(0, \Omega) &= v^0, \quad \frac{dE_{xh}}{dt}(0, \Omega) = v_t^0, \\ E_{xh}(t, \partial\Omega) &= v^{\text{bd}}, \quad \frac{dE_{xh}}{dt}(t, \partial\Omega) = v_t^{\text{bd}}, \end{aligned} \quad (4.10)$$

where $\mathbf{A} = \langle\langle \mathbf{A}_\Delta \rangle\rangle$. Hence, we have the equality

$$\frac{d^2 E_{xh}(t_k)}{dt^2} = \mathbf{A} E_{xh}(t_k) + f_h(t_k), \quad 2 \leq k \leq N. \quad (4.11)$$

Define the error function $e_h(t) = E_{xh}(t) - E_x(t, \mathbf{x}_h)$ with j -th components $e_j(t) := (e_h(t))_j$, where \mathbf{x}_h is a grid point. Using (4.11) and (2.7), we conclude that the error satisfies, for $2 \leq k \leq N$,

$$\frac{d^2 e_h(t_k)}{dt^2} = \mathbf{A} e_h(t_k) + r(t_k), \quad r(t_k) = \mathbf{A} E_x(t_k, \mathbf{x}_h) - \Delta E_x(t_k, \mathbf{x}_h). \quad (4.12)$$

We define

$$\Theta_h := \begin{bmatrix} e_1(t_h) \\ e_2(t_h) \\ \vdots \\ e_{N_{\text{int}}^{\text{dof}}}(t_h) \end{bmatrix}_{N_{\text{int}}^{\text{dof}} \times 1}, \quad \mathbf{R}_h := \begin{bmatrix} r_1(t_h) \\ r_2(t_h) \\ \vdots \\ r_{N_{\text{int}}^{\text{dof}}}(t_h) \end{bmatrix}_{N_{\text{int}}^{\text{dof}} \times 1},$$

where $r_j(t) = (r(t))_j$. Then, following [24, 23, 22], we deduce that

$$\mathbf{A}_{\text{Lap}} \Theta_h = \mathbf{R}_h,$$

with $|\mathbf{R}_h|_\infty \leq CN^4 e^{-CN}$ for some positive constant C , where \mathbf{A}_{Lap} is given in (3.7). Hence, by [23, Theorem 3.9] and the bounds on \mathbf{A}_{Lap} from the previous subsection, we obtain the desired error estimate. \square

Next, we focus on the convergence of the magnetic field variable \mathbf{B} .

Theorem 4.4. *Let (\mathbf{E}, \mathbf{B}) be the solution of the Maxwell system (2.1)–(2.4) (equivalently, let \mathbf{E} solve the vector wave equation (2.6) and \mathbf{B} be defined by (2.10)). Assume that both the electric field \mathbf{E} and the magnetic field \mathbf{B} are analytic functions in t, x, y , and z . Let Γ_h be the error associated with the collocation approximation of \mathbf{B} . Then*

$$|W^{1/2} \Gamma_h|_2 \leq c N^7 e^{-CN}. \quad (4.13)$$

Proof. Following the arguments in Theorem 4.3 and [23, Theorem 3.9], we derive

$$\mathbf{D}_t \Gamma_h = \tilde{\mathbf{R}}_h, \quad (4.14)$$

with $|\tilde{\mathbf{R}}_h|_\infty \leq CN^{6.5} e^{-CN}$, where C is a positive constant. Then, using the technique described in [24], we obtain the desired result. \square

The advantage of the proposed method is that we compute the magnetic field as $\mathbf{B}_h(t, \mathbf{x}) = \nabla_h \times \mathbf{E}_h(t, \mathbf{x})$, where $\mathbf{E}_h(t, \mathbf{x})$ is the discrete electric field. This approach does not enforce the divergence-free constraint of the electric field \mathbf{E}_h explicitly. However, we have the discrete identity $\nabla_h \cdot (\nabla_h \times \cdot) \approx 0$ and, consequently, the divergence-free condition for the magnetic field is satisfied asymptotically. Furthermore, we also highlight that the Gauss law for the electric field, $\|\nabla \cdot \mathbf{E}_h(t, \mathbf{x}) - \rho\|_{0,\Omega}$, converges to zero asymptotically.

The next theorem formalizes these observations by showing that the quantities $\nabla \cdot \mathbf{E} - \rho$ and $\nabla \cdot \mathbf{B}$ are not exactly zero but converge to zero with exponential rate.

Theorem 4.5. *Let (\mathbf{E}, \mathbf{B}) be the solution of the Maxwell system (2.1)–(2.4). Assume that both the electric field \mathbf{E} and the magnetic field \mathbf{B} are analytic functions in t, x, y , and z . Further, assume*

that \mathbf{E}_h and \mathbf{B}_h are the solutions of (2.25) and (3.8), respectively. Then the following estimates hold:

$$\|\nabla \cdot \mathbf{E}_h - \rho_h\|_{0,\Omega} \leq c N^{6.5} e^{-CN},$$

and

$$\|\nabla \cdot \mathbf{B}_h\|_{0,\Omega} \leq c N^9 e^{-CN}.$$

Proof. A straightforward calculation yields

$$\begin{aligned} \|\nabla \cdot \mathbf{E}_h - \rho_h\|_{0,\Omega} &\leq \|\nabla \cdot \mathbf{E}_h - \nabla \cdot \mathbf{E}\|_{0,\Omega} + \|\rho - \rho_h\|_{0,\Omega} \\ &\leq \|\mathbf{E}_h - \mathbf{E}\|_{1,\Omega} + \|\rho - \rho_h\|_{0,\Omega} \\ &\leq cN^2 \|\mathbf{E}_h - \mathbf{E}\|_{0,\Omega} + \|\rho - \rho_h\|_{0,\Omega} \\ &\leq cN^{6.5} e^{-CN} + ce^{-CN} \\ &\leq cN^{6.5} e^{-CN}. \end{aligned} \tag{4.15}$$

Following the same arguments, we rewrite the estimate for the magnetic field as

$$\begin{aligned} \|\nabla \cdot \mathbf{B}_h\|_{0,\Omega} &\leq \|\nabla \cdot \mathbf{B}_h - \nabla \cdot \mathbf{B}\|_{0,\Omega} \\ &\leq C\|\mathbf{B}_h - \mathbf{B}\|_{1,\Omega} \\ &\leq CN^2 \|\mathbf{B}_h - \mathbf{B}\|_{0,\Omega} \leq CN^2 N^7 e^{-CN} = CN^9 e^{-CN}, \end{aligned} \tag{4.16}$$

where we have used Theorem 4.3 and Theorem 4.4, together with the inverse estimate provided in [24, Section 2]. \square

In the next section, we describe the tensor-train modification of the full-grid scheme.

5. Tensor networks

In this section, we introduce the TT format, the specific tensor network we use in this work, the representation of linear operators in TT-matrix format, and the cross-interpolation method. All these methods are fundamental in the tensorization of our spectral collocation discretization of the Maxwell equations. For a more comprehensive understanding of notation and concepts, we refer the reader to the following references: Refs. [9, 19, 32], which provide detailed explanations.

5.1. Tensor train representation

The TT format, introduced by Oseledets in 2011 [32], represents a sequential chain of matrix products involving both two-dimensional matrices and three-dimensional tensors, referred to as TT-cores. We can visualize this chain as in Figure 1. Given that tensors in our formulation are at most four-dimensional (one temporal and three spatial dimensions), we consider the tensor train format in the context of 4D tensors. Specifically, the TT approximation \mathcal{X}^{TT} of a four-dimensional tensor \mathcal{X} is a tensor with elements

$$\mathcal{X}^{TT}(i_1, i_2, i_3, i_4) = \sum_{\alpha_1=1}^{r_1} \sum_{\alpha_2=1}^{r_2} \sum_{\alpha_3=1}^{r_3} \mathcal{G}_1(1, i_1, \alpha_1) \mathcal{G}_2(\alpha_1, i_2, \alpha_2) \mathcal{G}_3(\alpha_2, i_3, \alpha_3) \mathcal{G}_4(\alpha_3, i_4, 1) + \varepsilon, \tag{5.1}$$

where the error ε is a tensor with the same dimensions as \mathcal{X} , and the elements of the array $\mathbf{r} = [r_1, r_2, r_3]$ are the TT-ranks, which quantify the compression effectiveness of the TT approximation. Since each TT core \mathcal{G}_p only depends on a single index of the full tensor \mathcal{X} (e.g. i_k), the TT format effectively embodies a discrete separation of variables [4]. In Figure 1 we show a four-dimensional array $\mathcal{X}(t, x, y, z)$ decomposed in TT-format.

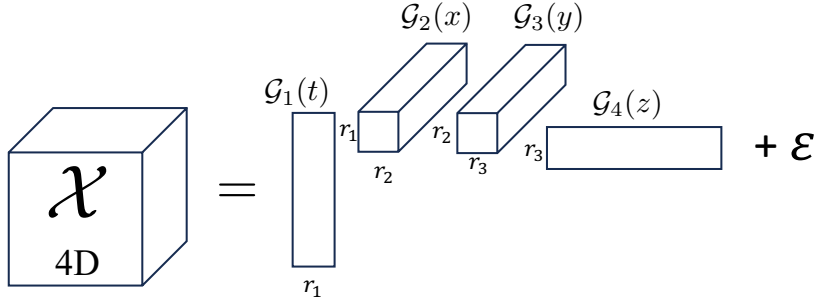


Figure 1: TT decomposition of a 4D tensor \mathcal{X} , with TT-rank $\mathbf{r} = [r_1, r_2, r_3]$ and approximation error ε , in accordance with Eq. (5.1).

5.2. Linear operators in TT-matrix format

Suppose that the approximate electric field solution of (2.7) is represented as a 4D tensor \mathcal{V} . Then the linear operator \mathcal{A} acting on that solution is represented as an 8D tensor. The transformation $\mathcal{A}\mathcal{V}$ is defined as:

$$(\mathcal{A}\mathcal{V})(i_1, i_2, i_3, i_4) = \sum_{j_1, j_2, j_3, j_4} \mathcal{A}(i_1, j_1, \dots, i_4, j_4) \mathcal{V}(j_1, \dots, j_4).$$

The tensor \mathcal{A} and the matrix operator \mathbf{A}_{Lap} , defined in Eq. (3.7), are related as:

$$\mathcal{A}(i_1, j_1, \dots, i_4, j_4) = \mathbf{A}_{Lap}(i_1 i_2 i_3 i_4, j_1 j_2 j_3 j_4). \quad (5.2)$$

Thus, we can construct the tensor \mathcal{A} by suitably reshaping and permuting the dimensions of the matrix \mathbf{A}_{Lap} . The linear operator \mathcal{A} can be further represented in a variant of TT format, called *TT-matrix*, cf. [38]. The component-wise TT-matrix \mathcal{A}^{TT} is defined as:

$$\mathcal{A}^{TT}(i_1, j_1, \dots, i_4, j_4) = \sum_{\alpha_1, \alpha_2, \alpha_3} \mathcal{G}_1(1, (i_1, j_1), \alpha_1) \dots \mathcal{G}_4(\alpha_3, (i_4, j_4), 1), \quad (5.3)$$

where \mathcal{G}_k are 4D TT-cores. Figure 2 shows the process of transforming a matrix operator \mathbf{A}_{Lap} to

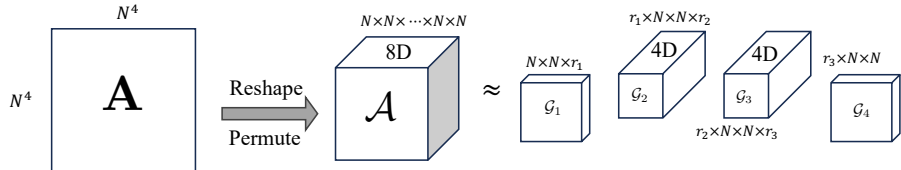


Figure 2: Representation of a linear matrix \mathbf{A}_{Lap} in the TT-matrix format. First, we reshape the operator matrix \mathbf{A}_{Lap} and permute its indices to create the tensor \mathcal{A} . Then, we factorize the tensor in the tensor-train matrix format according to Eq. (5.3) to obtain \mathcal{A}^{TT} .

its tensor format \mathcal{A} and, finally, to its TT-matrix format \mathcal{A}^{TT} .

We can further simplify the TT-matrix representations of the matrix \mathbf{A}_{Lap} if it is a Kronecker product of matrices, i.e. $\mathbf{A}_{Lap} = \mathbf{A}_1 \otimes \mathbf{A}_2 \otimes \mathbf{A}_3 \otimes \mathbf{A}_4$. Based on the relationship defined in Eq. (5.2), the tensor \mathcal{A} can be constructed using tensor products as $\mathcal{A} = \mathbf{A}_1 \circ \mathbf{A}_2 \circ \mathbf{A}_3 \circ \mathbf{A}_4$. This implies that the internal ranks of the TT-format of \mathcal{A} in (5.3) are all equal to 1. In such a case, all summations in Eq. (5.3) reduce to a sequence of single matrix–matrix multiplications, and the TT format of \mathcal{A} becomes the tensor product of d matrices:

$$\mathcal{A}^{TT} = \mathbf{A}_1 \circ \mathbf{A}_2 \circ \dots \circ \mathbf{A}_d. \quad (5.4)$$

This specific structure appears quite often in the matrix discretization and will be exploited in the tensorization to construct efficient TT representations.

5.3. TT cross interpolation

The original TT algorithm is based on consecutive applications of singular value decompositions (SVDs) on unfoldings of a tensor [32]. Although known for its efficiency, the TT algorithm requires access to the full tensor, which is impractical and even impossible for extra-large tensors. To address this challenge, the cross interpolation algorithm, TT-cross, has been developed [31]. The idea behind TT-cross is essentially to replace the SVD in the TT algorithm with an *approximate* version of the skeleton/CUR decomposition [13, 25]. CUR decomposition approximates a matrix by selecting a few of its columns \mathbf{C} , a few of its rows \mathbf{R} , and a matrix \mathbf{U} that connects them. Mathematically, CUR decomposition finds an approximation for a matrix \mathbf{A} as $\mathbf{A} \approx \mathbf{C}\mathbf{U}\mathbf{R}$. The TT-cross algorithm utilizes the maximum volume principle (*maxvol algorithm*) [12, 27] to determine \mathbf{U} . The maxvol algorithm chooses a few columns \mathbf{C} and rows \mathbf{R} of \mathbf{A} such that the intersection matrix \mathbf{U}^{-1} has maximum volume [35].

TT-cross interpolation and its variants can be seen as heuristic generalizations of CUR to tensors [34, 37]. TT-cross utilizes the maximum volume algorithm iteratively, often beginning with a few randomly chosen fibers, to select an optimal set of specific tensor fibers that capture the essential information of the tensor [36]. These fibers are used to construct a lower-rank TT representation. The naive generalization of CUR is known to be expensive, which has led to the development of various heuristic optimization techniques such as TT-ALS [15], DMRG [33, 35], and AMEN [10]. To solve the Maxwell equation in space-time format, we use TT-cross to build the TT format directly from the boundary conditions, initial conditions, and loading functions.

5.4. Tensorization of the electric field

From Section 3, we can immediately identify the core tensors for the TT-modification of the space-time discrete system. The space-time discretization produces a linear system for all interior nodes as specified in Eq. (3.7). Here, we simplify the notation and refer to this equation in the compact form $\mathbf{A}_{Lap}\mathbf{V} = \mathbf{F} - \mathbf{F}^{BD}$, where $\mathbf{V} = \hat{\mathbf{v}}_h$ collects the interior unknowns corresponding to the electric field component under consideration. Tensorization is the process of building the TT format of all components of this linear system,

$$\mathbf{A}_{Lap}\mathbf{V} = \mathbf{F} - \mathbf{F}^{BD} \longrightarrow \mathcal{A}^{TT}\mathcal{V}^{TT} = \mathcal{F}^{TT} - \mathcal{F}^{BD,TT}, \quad (5.5)$$

where $\mathcal{A}^{TT} = \mathcal{A}_t^{TT} + \mathcal{A}_D^{TT}$. In matrix form, the operator \mathbf{A}_{Lap} acts on the vectorized solution \mathbf{V} . In the full tensor format, the solution is kept in its original tensor form \mathcal{V} , which is a 4D tensor. Consequently, the operators \mathcal{A}_t and \mathcal{A}_D are 8D tensors. Lastly, \mathcal{F} and \mathcal{F}^{BD} are both 4D tensors. Given that these operators in matrix form have Kronecker product structure, their TT format can be constructed by using component matrices as TT cores. To construct the tensor format of the operators acting on the interior nodes, we define the index sets

$$\begin{aligned} \mathcal{I}_t &= 2 : N \quad (\text{index set for the time variable}), \\ \mathcal{I}_s &= 2 : (N - 1) \quad (\text{index set for each spatial variable}). \end{aligned}$$

- **TT-matrix time operator \mathcal{A}_t^{TT} :** The temporal operator in TT-matrix format acting only on the interior nodes is constructed as:

$$\mathcal{A}_t^{TT} = \mathbf{I}_{N-1} \circ \mathbf{I}_{N-1} \circ \mathbf{I}_{N-1} \circ \mathbf{S}_t(\mathcal{I}_t, \mathcal{I}_t), \quad (5.6)$$

where \mathbf{I}_{N-1} is the identity matrix of size $(N - 1) \times (N - 1)$.

- **TT-matrix diffusion operator \mathcal{A}_D^{TT} :** The Laplace operator in TT-matrix format is constructed as:

$$\begin{aligned}\mathcal{A}_D^{TT} = & \mathbf{S}_{xx}(\mathcal{I}_s, \mathcal{I}_s) \circ \mathbf{I}_{N-1} \circ \mathbf{I}_{N-1} \circ \mathbf{I}_N + \mathbf{I}_{N-1} \circ \mathbf{S}_{yy}(\mathcal{I}_s, \mathcal{I}_s) \circ \mathbf{I}_{N-1} \circ \mathbf{I}_N \\ & + \mathbf{I}_{N-1} \circ \mathbf{I}_{N-1} \circ \mathbf{S}_{zz}(\mathcal{I}_s, \mathcal{I}_s) \circ \mathbf{I}_N.\end{aligned}\quad (5.7)$$

- **TT loading tensor \mathcal{F}^{TT} :** The TT loading tensor \mathcal{F}^{TT} is constructed by applying TT-cross interpolation to the function $f(t, x, y, z)$ on the grid of interior nodes. Such techniques are investigated in [2, 1]. We highlight that if the forcing term satisfies a *separation-of-variables* condition, cross interpolation may not be necessary to construct the loading tensor.

- **TT boundary tensor $\mathcal{F}^{BD,TT}$:** Unlike full-grid computation, the implementation of boundary conditions for a tensor-train grid is not straightforward. In this direction, we construct an operator \mathcal{A}^{map} which imposes the given boundary and initial data at the correct positions. In particular, \mathcal{A}^{map} maps all nodes to the subset of unknown nodes. The size of the operator \mathcal{A}^{map} is $(N-2) \times (N) \times (N-1) \times (N+1) \times (N-1) \times (N+1) \times (N) \times (N+1)$ according to the . Here, odd indices signify only the number of unknown nodes, while even indices signify the total number of nodes. The boundary tensor \mathcal{F}^{BD} is then computed by applying \mathcal{A}^{map} to a tensor \mathcal{G}^{BD} containing only the information from boundary and initial conditions. The details about constructing $\mathcal{A}^{map,TT}$ and $\mathcal{G}^{BD,TT}$ are included in [Appendix A](#). Here, we focused on the tensorization of E_x variable corresponding to (2.7). The tensorization for other components such as E_y , and E_z will be followed same technique as mentioned above.

At this point, we have completed the construction of the TT-format of the linear system $\mathcal{A}^{TT}\mathcal{V}^{TT} = \mathcal{F}^{TT} - \mathcal{F}^{BD,TT}$. To solve this TT linear system by optimization techniques, we use the routines `amen_cross`, `amen_solve` and `amen_mm` from the MATLAB TT-Toolbox [30].

5.5. Tensorization of the magnetic field

In this section, we primarily focus on the TT format of the magnetic-field component B_{xh} in (3.8); the computation of the other components B_{yh} and B_{zh} is analogous. The TT-modification of the interior system (3.11) can be written as

$$\mathcal{A}_t^{TT}\mathcal{B}_x^{TT} = \mathcal{F}_{\text{curl}}^{TT} - \mathcal{F}_{\text{curl}}^{BD,TT}, \quad (5.8)$$

where \mathcal{A}_t^{TT} is defined in (5.6), and \mathcal{B}_x^{TT} is the 4D tensor representing the magnetic-field component B_{xh} . Further, $\mathcal{F}_{\text{curl}}^{TT}$ is a 4D tensor computed as

$$\begin{aligned}\mathcal{F}_{\text{curl}}^{TT} = & \left(\mathbf{I}_x(\mathcal{I}_s, \mathcal{I}_s) \circ \mathbf{S}_y(\mathcal{I}_s, \mathcal{I}_s) \circ \mathbf{I}_z(\mathcal{I}_s, \mathcal{I}_s) \circ \mathbf{I}_t(\mathcal{I}_t, \mathcal{I}_t) \right) \mathcal{I}_{V_z \rightarrow S_x} \mathbf{E}_z \\ & - \left(\mathbf{I}_x(\mathcal{I}_s, \mathcal{I}_s) \circ \mathbf{I}_y(\mathcal{I}_s, \mathcal{I}_s) \circ \mathbf{S}_z(\mathcal{I}_s, \mathcal{I}_s) \circ \mathbf{I}_t(\mathcal{I}_t, \mathcal{I}_t) \right) \mathcal{I}_{V_y \rightarrow S_x} \mathbf{E}_y,\end{aligned}\quad (5.9)$$

where $\mathcal{I}_{V_z \rightarrow S_x}$ is the matrix corresponding to the interpolation operator that maps the vector of collocation values \mathbf{E}_z to the grid associated with V_k^x in (2.22). Similarly, $\mathcal{I}_{V_y \rightarrow S_x}$ maps the vector \mathbf{E}_y to the grid corresponding to V_k^x . We highlight that this interpolation operator is needed since we have computed the electric and magnetic field components on different staggered grids. In this post-processing technique, one must also treat boundary nodes carefully; this can be done following the techniques in [2].

Further, we need to tensorize the boundary term $\mathcal{F}_{\text{curl}}^{BD,TT}$, which is given by

$$\mathcal{F}_{\text{curl}}^{BD,TT} = \mathbf{I}_x(\mathcal{I}_s, :) \circ \mathbf{I}_y(\mathcal{I}_s, :) \circ \mathbf{I}_z(\mathcal{I}_s, :) \circ \mathbf{S}_t(\mathcal{I}_t, :) \mathcal{G}_{B_x}^{BD,TT}, \quad (5.10)$$

where $\mathcal{G}_{B_x}^{BD,TT}$ is the $(N+1) \times N \times N \times (N+1)$ boundary tensor that consists only of boundary and initial values and zeros at the interior grid points. For a more detailed discussion, we refer to [1, 32] and [Appendix A](#).

6. Numerical Experiments

In this section, we present numerical experiments that assess the performance of our tensor-network-based space–time spectral collocation method for Maxwell’s equations in Tensor-Train (TT) format. The first two tests use manufactured solutions of rank 1, while the third test considers a rank 3 solution. In all experiments, the tolerance used in the TT truncation is chosen to be smaller than the approximation error introduced when constructing the TT representation. Throughout, we compare the TT-based solver with a full-grid solver that operates directly on dense tensors. All simulations are performed in MATLAB on a Mac system with an M2 processor.

6.1. Experiment 1

In the first test, we apply the TT-solver to (2.1)–(2.4) using the manufactured solution

$$\mathbf{E}(\mathbf{x}, t) = \begin{bmatrix} 0 \\ \sin(2\pi x) \sin(2\pi y) \sin(2\pi t) \\ \sin(\pi x) \sin(\pi y) \cos(\pi t) \end{bmatrix}, \quad \mathbf{B}(\mathbf{x}, t) = \begin{bmatrix} -\sin(\pi x) \cos(\pi y) \sin(\pi t) \\ \cos(\pi x) \sin(\pi y) \sin(\pi t) \\ \cos(2\pi x) \sin(2\pi y) \cos(2\pi t) \end{bmatrix}. \quad (6.1)$$

The computational domain is $\Omega_T = [0, 1] \times [0, 1]^3$, with $\epsilon_0 = 1$ and $c = 1$. The exact solution is independent of the z -variable, and boundary and initial data are chosen accordingly.

The TT-solver matches the accuracy of the full-grid solver, reaching errors on the order of 10^{-10} with 22 grid points per dimension when using a TT tolerance of 10^{-11} . The convergence behaviour is illustrated in Figure 3: the upper-left panel shows the L_2 -errors in the electric and magnetic fields as a function of the number of grid points, while the upper-right panel shows the corresponding divergence errors $\|\operatorname{div} \mathbf{E} - \rho\|$ and $\|\operatorname{div} \mathbf{B}\|$. The divergence of the magnetic field converges exponentially to zero, consistent with the fact that \mathbf{B} is computed in the curl space of \mathbf{E} and $\operatorname{div}(\operatorname{curl} \cdot) = 0$, and Gauss’s law for \mathbf{E} is also satisfied with exponential accuracy. These observations confirm the theoretical results of Theorem 4.5.

Finally, we highlight the difference in computational cost. The bottom panel of Figure 3 compares the elapsed time of the TT-based and full-grid solvers. While both solvers initially require comparable time, the full-grid solver becomes significantly more expensive as the grid is refined; for example, at 22 points per dimension the TT-solver is approximately 10^7 times faster.

6.2. Experiment 2

In the second experiment, we again study (2.1)–(2.4), now with a three-dimensional manufactured solution:

$$\mathbf{E}(\mathbf{x}, t) = \begin{bmatrix} 0 \\ \sin(2\pi x) \sin(2\pi y) \sin(2\pi z) \sin(2\pi t) \\ \sin(\pi x) \sin(\pi y) \sin(\pi z) \cos(\pi t) \end{bmatrix}, \quad (6.2)$$

$$\mathbf{B}(\mathbf{x}, t) = \begin{bmatrix} -\sin(\pi x) \cos(\pi y) \sin(\pi z) \sin(\pi t) - \sin(2\pi x) \sin(2\pi y) \cos(2\pi z) \cos(2\pi t) \\ \cos(\pi x) \sin(\pi y) \sin(\pi z) \sin(\pi t) \\ \cos(2\pi x) \sin(2\pi y) \sin(2\pi z) \cos(2\pi t) \end{bmatrix}. \quad (6.3)$$

The domain is $\Omega_T = [0, 1] \times [-1, 1]^3$ with $\epsilon_0 = 1$ and $c = 1$. Initial and boundary data are derived from the exact solution.

The TT-solver again reproduces the accuracy of the full-grid solver on coarse and moderate grids (see Figure 4). Beyond 12 points per dimension, the full-grid method exceeds available memory, whereas the TT-solver remains efficient and stable up to at least 22 points per dimension.

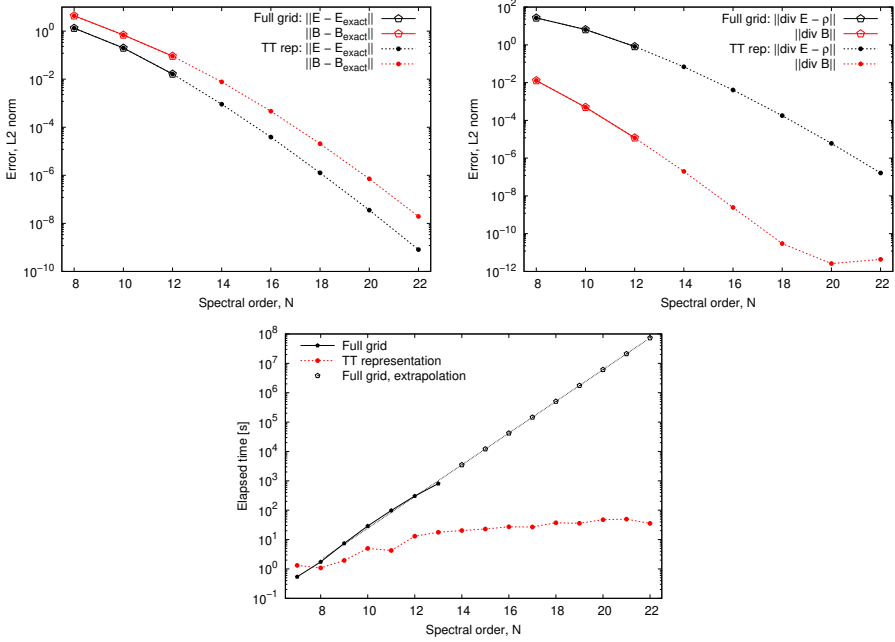


Figure 3: Test Case 1, upper panels: L_2 -errors in the computation of the electric and magnetic fields (upper left), and divergence constraints: $\|\operatorname{div} \mathbf{E} - \rho\|$, $\|\operatorname{div} \mathbf{B}\|$ (upper right). Bottom panel: elapsed time for the full grid calculation vs TT representation.

The divergence of \mathbf{B} converges exponentially to zero, and Gauss's law for \mathbf{E} is satisfied with the same rate, again matching the theoretical predictions of Theorem 4.5.

Timing results in Figure 4 show the full-grid solver scaling steeply with grid size, while the TT-based solver exhibits a much milder growth in cost. Extrapolation of full-grid timings indicates that for a 24-point grid, the TT-solver is roughly 10^8 times faster.

6.3. Experiment 3

The third test considers a higher-rank solution:

$$\mathbf{E}(\mathbf{x}, t) = \begin{bmatrix} 0 \\ 0 \\ \sum_{k=1}^3 \sin(k\pi x) \sin(k\pi y) \cos(k\pi t) \end{bmatrix}, \quad \mathbf{B}(\mathbf{x}, t) = \begin{bmatrix} -\sum_{k=1}^3 \sin(k\pi x) \cos(k\pi y) \sin(k\pi t) \\ \sum_{k=1}^3 \cos(k\pi x) \sin(k\pi y) \sin(k\pi t) \\ 0 \end{bmatrix}. \quad (6.4)$$

Boundary and initial conditions are taken from the exact expressions. This experiment evaluates performance when the true solution has higher tensor rank.

The TT- and full-grid solvers deliver comparable accuracy across all tested grid sizes (see Figure 5). As in the previous experiments, both methods require similar computational effort on coarse grids, but the full-grid cost grows rapidly with refinement. At 22 grid points per dimension, the TT-solver is about 10^7 times faster than the full-grid method. These results confirm that the TT approach remains effective even for solutions with higher intrinsic rank, and that it is well suited for large-scale Maxwell simulations involving many variables.

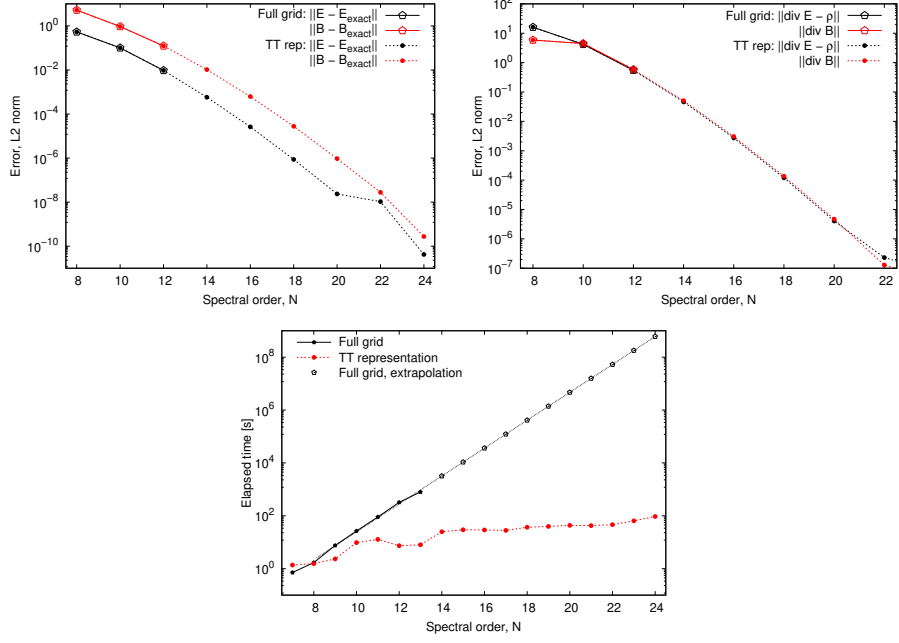


Figure 4: Test Case 2, upper panels: L_2 -errors of electric and magnetic fields (upper left), and divergence constraints: $\| \operatorname{div} \mathbf{E} - \rho \|$, $\| \operatorname{div} \mathbf{B} \|$ (upper right). Bottom panel: elapsed time for full grid calculation vs TT representation.

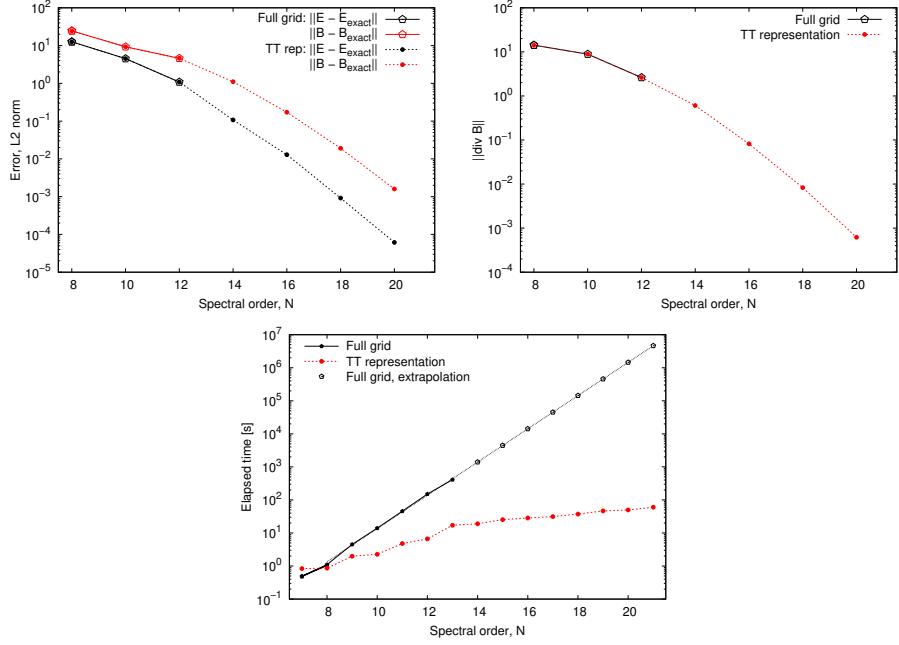


Figure 5: Test Case 3, upper panels: L_2 -error in the computation of the electric and magnetic fields (upper left), and divergence constraint $\operatorname{div} \mathbf{B} = 0$ (upper right). Bottom panel: elapsed time for full-grid calculation vs. TT representation.

7. Conclusions

In this work, we have developed and analyzed a space-time spectral collocation tensor network method for the efficient numerical solution of Maxwell’s equations in three spatial dimensions. Our approach combines the exponential convergence properties of Chebyshev spectral methods with the dimensional scalability of tensor-train decomposition, addressing the curse of dimensionality that has long hindered high-resolution electromagnetic simulations.

The key contributions of this work are threefold. First, we have formulated a space-time spectral collocation scheme that discretizes both spatial and temporal dimensions using Chebyshev polynomials, yielding a global system that captures the entire time evolution simultaneously. By reformulating Maxwell’s equations as a second-order wave equation for the electric field under constant-coefficient assumptions, we decouple the system into independent componentwise problems with natural Kronecker product structure. Second, we have introduced a staggered spectral discretization where electric and magnetic field components live in different polynomial spaces with carefully chosen degrees of freedom in each coordinate direction. This spectral staggering preserves the divergence-free property of the magnetic field to spectral accuracy without explicit constraint enforcement, analogous to classical FDTD staggering but within a high-order spectral framework. Third, we have developed a complete tensorization strategy that exploits the Kronecker structure of the discrete operators to construct efficient tensor-train representations using TT-cross interpolation and alternating minimal energy solvers.

Our theoretical analysis establishes rigorous foundations for the method. We have derived condition number estimates showing that the discrete wave operator scales as $\mathcal{O}(N^4)$ while the temporal operator for magnetic field reconstruction scales as $\mathcal{O}(N^2)$, where N is the polynomial degree. More importantly, we have proven exponential convergence of the discrete electric and magnetic fields in the L^2 norm, with convergence rates of the form $\mathcal{O}(N^p e^{-CN})$ for appropriate powers p . Furthermore, we have established that both Gauss’s law for the electric field and the divergence-free constraint for the magnetic field are satisfied with exponential accuracy, confirming that the discrete divergence operator applied to the discrete curl vanishes asymptotically.

Numerical experiments validate these theoretical results and demonstrate the practical efficiency of the method. Across three test cases with manufactured solutions of varying tensor rank, we consistently observe exponential convergence matching the full-grid spectral method while achieving dramatic computational savings. For problems with 22 collocation points per dimension (corresponding to approximately 10^8 degrees of freedom in the space-time grid), the tensor-train solver is roughly 10^7 times faster than the full-grid approach. Critically, the TT method extends beyond the memory limitations of full-grid computation: while full-grid methods become infeasible beyond 12–14 points per dimension, the TT solver successfully handles 22–24 points, accessing a regime that would be completely intractable with conventional approaches.

Our work demonstrates that space-time spectral collocation methods, when combined with tensor-train compression, provide a powerful tool for solving Maxwell’s equations with unprecedented efficiency and accuracy. By achieving exponential convergence while maintaining linear complexity in storage and computation, the method opens new possibilities for high-fidelity electromagnetic simulations that were previously computationally prohibitive. The rigorous mathematical framework, validated through numerical experiments, establishes a solid foundation for further developments in tensor network methods for computational electromagnetics.

Appendix A. Construction of $\mathcal{A}^{map,TT}$ and \mathcal{G}^{TT} [1]

Here we provide details about the construction of $\mathcal{A}_{E_x}^{map,BD}$, $\mathcal{A}_{E_x}^{map,IC}$, $\mathcal{A}_{E_{x,t}}^{map,BD}$, $\mathcal{A}_{E_{x,t}}^{map,IC}$ and $\mathcal{G}_{E_x}^{BD,TT}$, $\mathcal{G}_{E_x}^{IC,TT}$, $\mathcal{G}_{E_{x,t}}^{BD,TT}$, $\mathcal{G}_{E_{x,t}}^{IC,TT}$, where BD , and IC stand for boundary condition and initial condition in space and time variables respectively. The sub-index E_x , and $E_{x,t}$ signify implementation boundary condition or initial guess for E_x , and $\frac{\partial E_x}{\partial t}$ respectively. We define

$$\begin{aligned}\mathcal{A}_1^{map} &= \mathbf{I}^{N+1}(\mathcal{I}_s, \mathcal{I}_s) \circ \mathbf{I}^{N+1}(\mathcal{I}_s, \mathcal{I}_s) \circ \mathbf{I}^{N+1}(\mathcal{I}_s, \mathcal{I}_s) \circ \mathbf{S}_t(\mathcal{I}_t, \mathcal{I}_t), \\ \mathcal{A}_2^{map} &= \mathbf{I}^{N+1}(\mathcal{I}_s, :) \circ \mathbf{I}^{N+1}(\mathcal{I}_s, :) \circ \mathbf{I}^{N+1}(\mathcal{I}_s, :) \circ \mathbf{S}_t(\mathcal{I}_t, :), \\ \mathcal{A}_3^{map} &= \mathbf{I}^{N+1}(\mathcal{I}_s, :) \circ \mathbf{I}^{N+1}(\mathcal{I}_s, :) \circ \mathbf{I}^{N+1}(\mathcal{I}_s, :) \circ \mathbf{I}^{N+1}(\mathcal{I}_t, :), \\ \mathcal{A}_4^{map} &= \mathbf{S}_{xx}(\mathcal{I}_s, :) \circ \mathbf{I}^{N+1}(\mathcal{I}_s, :) \circ \mathbf{I}^{N+1}(\mathcal{I}_s, :) \circ \mathbf{I}^{N+1}(\mathcal{I}_t, :) \\ &\quad + \mathbf{I}^{N+1}(\mathcal{I}_s, :) \circ \mathbf{S}_{yy}(\mathcal{I}_s, :) \circ \mathbf{I}^{N+1}(\mathcal{I}_s, :) \circ \mathbf{I}^{N+1}(\mathcal{I}_t, :) \\ &\quad + \mathbf{I}^{N+1}(\mathcal{I}_s, :) \circ \mathbf{I}^{N+1}(\mathcal{I}_s, :) \circ \mathbf{S}_{zz}(\mathcal{I}_s, :) \circ \mathbf{I}^{N+1}(\mathcal{I}_t, :).\end{aligned}\tag{A.1}$$

By using (A.1), we construct the final mapping as follows

$$\begin{aligned}\mathcal{A}_{E_x}^{map,BD} &= \mathcal{A}_4^{map}, & \mathcal{A}_{E_x}^{map,IC} &= \mathcal{A}_1^{map} \mathcal{A}_2^{map}, \\ \mathcal{A}_{E_{x,t}}^{map,BD} &= \mathcal{A}_1^{map} \mathcal{A}_3^{map}, & \mathcal{A}_{E_{x,t}}^{map,IC} &= \mathcal{A}_2^{map}.\end{aligned}\tag{A.2}$$

Next, we show how to construct the \mathcal{G}^{BD} tensor. The tensor \mathcal{G}^{BD} is a $(N) \times (N+1) \times (N+1) \times (N+1)$, in which only the BD/IC nodes are computed. Other nodes are zeros. The TT tensor \mathcal{G}^{BD} is constructed using the cross interpolation. Then, the boundary tensor $\mathcal{F}^{BD,TT}$ is computed as:

$$\mathcal{F}^{BD,TT} = \mathcal{A}_{E_x}^{map,BD} \mathcal{G}_{E_x}^{BD,TT} + \mathcal{A}_{E_x}^{map,IC} \mathcal{G}_{E_x}^{IC,TT} + \mathcal{A}_{E_{x,t}}^{map,BD} \mathcal{G}_{E_{x,t}}^{BD,TT} + \mathcal{A}_{E_x}^{map,IC} \mathcal{G}_{E_x}^{IC,TT}.\tag{A.3}$$

Data availability statement

The data that support the findings of this research are available from the corresponding author upon reasonable request.

Declaration of competing interest

The authors declare that they have no known competing financial interests or personal relationships that could have appeared to influence the work reported in this paper.

CRediT authorship contribution statement

D. Adak, D. P. Truong, R. Chinomona, O. Korobkin, Kim O. Rasmussen, B. S. Alexandrov : Conceptualization, Methodology, Writing-original draft, Review & Editing.

Acknowledgments

The authors gratefully acknowledge the support of the Laboratory Directed Research and Development (LDRD) program of Los Alamos National Laboratory under project number 20240705ER. Los Alamos National Laboratory is operated by Triad National Security, LLC, for the National Nuclear Security Administration of U.S. Department of Energy (Contract No. 89233218CNA000001).

References

- [1] Dibyendu Adak, M Engin Danis, Duc P Truong, Kim Ø Rasmussen, and Boian S Alexandrov. Tensor network space-time spectral collocation method for solving the nonlinear convection diffusion equation. *Journal of Scientific Computing*, 103(2):46, 2025.
- [2] Dibyendu Adak, Duc P Truong, Gianmarco Manzini, Kim Ø Rasmussen, and Boian S Alexandrov. Tensor network space-time spectral collocation method for time-dependent convection-diffusion-reaction equations. *Mathematics*, 12(19):2988, 2024.
- [3] Adérito Araujo, Sílvia Barbeiro, and Maryam Khaksar Ghalati. Stability of a leap-frog discontinuous galerkin method for time-domain maxwell's equations in anisotropic materials. *Communications in Computational Physics*, 21(5):1350–1375, 2017.
- [4] M. Bachmayr, R. Schneider, and A. Uschmajew. Tensor networks and hierarchical tensors for the solution of high-dimensional partial differential equations. *Foundations of Computational Mathematics*, 16:1423–1472, 2016.
- [5] R. Bellman. Dynamic programming. *Science*, 153(3731):34–37, 1966.
- [6] Liliana Camargo, Bibiana López-Rodríguez, Mauricio Osorio, and Manuel Solano. An hdg method for maxwell's equations in heterogeneous media. *Computer Methods in Applied Mechanics and Engineering*, 368:113178, 2020.
- [7] P Collino, Gianluca Delbue, Patrick Joly, and Andrea Piacentini. A new interface condition in the non-overlapping domain decomposition method for the maxwell equations. *Computer methods in applied mechanics and engineering*, 148(1-2):195–207, 1997.
- [8] Engin Danis, Duc P. Truong, Kim Ø. Rasmussen, and Boian S Alexandrov. Tensor-train operator inference. *arXiv preprint arXiv:2509.08071*, 2025.
- [9] S. Dolgov and T. Vejchodský. Guaranteed a posteriori error bounds for low-rank tensor approximate solutions. *IMA Journal of Numerical Analysis*, 41(2):1240–1266, 2021.
- [10] S. V. Dolgov and D. V. Savostyanov. Alternating minimal energy methods for linear systems in higher dimensions. *SIAM Journal on Scientific Computing*, 36(5):A2248–A2271, 2014.
- [11] D. Funaro. *Spectral elements for transport-dominated equations*, volume 1. Springer Science & Business Media, 1997.
- [12] S. A. Goreinov, I. V. Oseledets, D. V. Savostyanov, E. E. Tyrtyshnikov, and N. L. Zamarashkin. How to find a good submatrix. In *Matrix Methods: Theory, Algorithms And Applications: Dedicated to the Memory of Gene Golub*, pages 247–256. World Scientific, 2010.
- [13] S. A. Goreinov, E. E. Tyrtyshnikov, and N. L. Zamarashkin. A theory of pseudoskeleton approximations. *Linear algebra and its applications*, 261(1-3):1–21, 1997.
- [14] Max D Gunzburger, Janet S Peterson, and John N Shadid. Reduced-order modeling of time-dependent pdes with multiple parameters in the boundary data. *Computer methods in applied mechanics and engineering*, 196(4-6):1030–1047, 2007.
- [15] S. Holtz, T. Rohwedder, and R. Schneider. The alternating linear scheme for tensor optimization in the tensor train format. *SIAM Journal on Scientific Computing*, 34(2):A683–A713, 2012.
- [16] Jianguo Huang and Shangyou Zhang. A divergence-free finite element method for a type of 3d maxwell equations. *Applied Numerical Mathematics*, 62(6):802–813, 2012.

- [17] M. Y. Hussaini, D. A. Kopriva, and A. T. Patera. Spectral collocation methods. *Applied Numerical Mathematics*, 5(3):177–208, 1989.
- [18] V. A. Kazeev, B. N. Khoromskij, and E. E. Tyrtyshnikov. Multilevel Toeplitz matrices generated by tensor-structured vectors and convolution with logarithmic complexity. *SIAM Journal on Scientific Computing*, 35(3):A1511–A1536, 2013.
- [19] T. G. Kolda and B. W. Bader. Tensor decompositions and applications. *SIAM review*, 51(3):455–500, 2009.
- [20] Jerome R Krebs, John E Anderson, David Hinkley, Ramesh Neelamani, Sunwoong Lee, Anatoly Baumstein, and Martin-Daniel Lacasse. Fast full-wavefield seismic inversion using encoded sources. *Geophysics*, 74(6):WCC177–WCC188, 2009.
- [21] Günter Leugering, Peter Benner, Sebastian Engell, Andreas Griewank, Helmut Harbrecht, Michael Hinze, Rolf Rannacher, and Stefan Ulbrich. *Trends in PDE constrained optimization*, volume 165. Springer, 2014.
- [22] SH. Lui. Legendre spectral collocation in space and time for pdes. *Numerische Mathematik*, 136(1):75–99, 2017.
- [23] SH Lui and Sarah Nataj. Chebyshev spectral collocation in space and time for the heat equation. *Electronic Transactions on Numerical Analysis*, 52:295–319, 2020.
- [24] SH Lui and Sarah Nataj. Spectral collocation in space and time for linear pdes. *Journal of Computational Physics*, 424:109843, 2021.
- [25] M. W. Mahoney and P. Drineas. CUR matrix decompositions for improved data analysis. *Proceedings of the National Academy of Sciences*, 106(3):697–702, 2009.
- [26] G Manzini, P. M. D. Truong, R Vuchkov, and B Alexandrov. The tensor-train mimetic finite difference method for three-dimensional Maxwell’s wave propagation equations. *Mathematics and Computers in Simulation*, 210:615–639, 2023.
- [27] A. Mikhalev and I. V. Oseledets. Rectangular maximum-volume submatrices and their applications. *Linear Algebra and its Applications*, 538:187–211, 2018.
- [28] Peter Monk. Analysis of a finite element method for maxwell’s equations. *SIAM Journal on Numerical Analysis*, 29(3):714–729, 1992.
- [29] Cuixia Niu, Heping Ma, and Dong Liang. Legendre-tau chebyshev collocation spectral element method for maxwell’s equations with material interfaces of two dimensional transverse magnetic mode. *Computers & Mathematics with Applications*, 147:222–238, 2023.
- [30] I. Oseledets. TT-Toolbox, Version 2.2, 2023. Available at <https://github.com/oseledets/TT-Toolbox>.
- [31] I. Oseledets and E. Tyrtyshnikov. TT-cross approximation for multidimensional arrays. *Linear Algebra and its Applications*, 432(1):70–88, 2010.
- [32] I. V. Oseledets. Tensor-train decomposition. *SIAM Journal on Scientific Computing*, 33(5):2295–2317, 2011.
- [33] I. V. Oseledets and S. V. Dolgov. Solution of linear systems and matrix inversion in the TT-format. *SIAM Journal on Scientific Computing*, 34(5):A2718–A2739, 2012.

- [34] I. V. Oseledets, D. V. Savostyanov, and E. E. Tyrtyshnikov. Tucker dimensionality reduction of three-dimensional arrays in linear time. *SIAM, Journal on Matrix Analysis and Applications*, 30(3):939–956, 2008.
- [35] D. Savostyanov and I. Oseledets. Fast adaptive interpolation of multi-dimensional arrays in tensor train format. In *The 2011 International Workshop on Multidimensional (nD) Systems*, pages 1–8. IEEE, 2011.
- [36] D. V. Savostyanov. Quasioptimality of maximum-volume cross interpolation of tensors. *Linear Algebra and its Applications*, 458:217–244, 2014.
- [37] K. Sozykin, A. Chertkov, R. Schutski, A.-H. Phan, A. S. Cichoki, and I. Oseledets. TTOpt: A maximum volume quantized tensor train-based optimization and its application to reinforcement learning. *Advances in Neural Information Processing Systems*, 35:26052–26065, 2022.
- [38] Duc P Truong, Mario I Ortega, Ismael Boureima, Gianmarco Manzini, Kim Ø Rasmussen, and Boian S Alexandrov. Tensor networks for solving the time-independent boltzmann neutron transport equation. *Journal of Computational Physics*, 507:112943, 2024.
- [39] Kane Yee. Numerical solution of initial boundary value problems involving maxwell’s equations in isotropic media. *IEEE Transactions on antennas and propagation*, 14(3):302–307, 1966.
- [40] A Yefet and E Turkel. Fourth order compact implicit method for the maxwell equations with discontinuous coefficients. *Applied Numerical Mathematics*, 33(1-4):125–134, 2000.
- [41] Amir Yefet and Peter G Petropoulos. A staggered fourth-order accurate explicit finite difference scheme for the time-domain maxwell’s equations. *Journal of Computational Physics*, 168(2):286–315, 2001.